The SWIRE Data Release 2: Image Atlases and Source Catalogs for ELAIS-N1, ELAIS-N2, XMM-LSS, and the Lockman Hole

J. A. Surace[1], D.L. Shupe[1], F. Fang[1], C.J. Lonsdale[2,3], E. Gonzalez-Solares[4], E. Hatziminaoglou[11], B. Siana[3], T. Babbedge[5], M. Polletta[2,3], G. Rodighiero[7], M. Vaccari[4], I. Waddington[6], S. Berta[7], D. Frayer[1], T. Evans[2], T. Jarrett[2], D.L. Padgett[1], S. Castro[15], F. Masci[1], D. Domingue[13], M. Pierre[8], M. Fox[5], M. Rowan-Robinson[5], I. Perez-Fournon[11], S. Oliver[6], G. Stacey[9], D. Farrah[2], H.E. Smith[3], A. Franceschini[7], F. Owen[10], C. Xu[2], A. Afonso-Luis[11], P. Davoodi[5], H. Dole[14], F. Pozzi[12], M. Salaman[6]

1. Overview: Products, Sky Coverage and Cautions

The Spitzer Wide-area InfraRed Extragalactic survey (SWIRE; Lonsdale et al. 2003) Version 2.0 data products release (hereafter also known as V2 or DR2) includes an image atlas and source catalogs for the first four of the six SWIRE fields to be observed by Spitzer: the ELAIS-N1, ELAIS-N2, XMM-LSS, and Lockman Hole fields. The release includes both Spitzer IRAC and MIPS mid/far-infrared data products for all four fields as well as Ug′ r′ i′ Z optical data covering selected subregions of the data (McMahon et al. 2001, Gonzalez-Solares et al. 2004). This document describes the data processing that the SWIRE team has undertaken to produce high-level data products from the basic data released by the Spitzer Science Center, and describes the products in detail. This data release supersedes the original version 1 data release of the ELAIS-N1 field, and the new products should now be used in place of the old ones. Section 2 details differences between the first and second data release.

[1]Spitzer Science Center, MS 220–6, California Institute of Technology, Jet Propulsion Laboratory, Pasadena, CA 91125, USA

[2]Infrared Processing and Analysis Center, MS 100-22, California Institute of Technology, Jet Propulsion Laboratory, Pasadena, CA 91125, USA

[3]Center for Astrophysics & Space Sciences, University of California San Diego, La Jolla, CA 92093-0424, USA

[4]Institute of Astronomy, University of Cambridge, Madingley Road, Cambridge, CB3 0HA, UK

[5]Astrophysics Group, Blackett Laboratory, Imperial College, Prince Consort Road, London, SW7 2BW, UK

[6]Astronomy Centre, Department of Physics & Astronomy, University of Sussex, Brighton, BN1 9QH, UK

[7]Dipartimento di Astronomia, Universita di Padova, Vicolo Osservatorio 5, I-35122 Padua, Italy

[8]CEA/DSM/DAPNIA, Service d'Astrophysique, 91191 Gif-sur-Yvette, France

[9]Department of Astronomy, Cornell University, 220 Space Science Building, Ithaca, NY 14853

[10]National Radio Astronomy Observatory, P.O. Box O, Socorro, NM 87801

[11]Instituto de Astrofisica de Canarias, 38200 La Laguna, Tenerife, Spain

[12]Universita degli Studi di Bologna, Dipartimento Astronomia di Bologna via Ranzani 1, 40127 Bologna, ITALY

[13]Department of Chemistry and Physics, Georgia College and State University, Milledgeville, GA, 31061

[14]Institut d'Astrophysique Spatiale, batiment 121, Universit Paris Sud, F-91405 Orsay Cedex, France

[15]European Southern Observatory Karl-Schwarzschildstr. 2 Garching bei Mnchen 85748 Germany

The Version 2.0 SWIRE Spitzer Image Atlas consists of sets of IRAC mosaicked "tiles", and MIPS images, one per band. Each IRAC tile has four FITS images, one per IRAC band. In addition we also provide for each band and each IRAC tile a noise image, a coverage image and a mask image. The released optical data is provided as a set of tiles matching the IRAC tiles, with the same image boundaries, projection, and rotation. Additionally, a set of pseudo-truecolor images made from the IRAC data are provided.

The Version 2.0 SWIRE Source Catalogs have four parts: (1) a catalog including IRAC and MIPS 24μm sources which have been bandmerged together. The Spitzer source list has been positionally matched to an optical source list (when available) and we report optical position and 5-band magnitude data for each successful match. This catalog contains only sources lying with the region which has full coverage in all four IRAC bands; (2) a 24μm only catalog, which has different selection criteria and contains some sources not selected in the combined optical-IRAC-MIPS catalog; (3) a 70μm catalog; and (4) a 160μm catalog. The longer wavelength catalogs have not been bandmerged with the IRAC+24μm catalog or the optical source list at this time because of complex source confusion issues. The three MIPS-Ge catalogs cover the full area scanned by each MIPS-array, except for areas of low coverage around each edge, and are not restricted to the full IRAC coverage area.

Users should note that the SWIRE releases are typically phased over several months. In general, image products become available first, followed by the combined optical-IRAC-MIPS catalogs, and finally the MIPS-only long wavelength catalogs. Users should consult the SSC and SWIRE web pages for exact details on data availability.

We summarize here some important cautions to be taken into account when using the SWIRE Release 2 Data Products, highlighted in **bold face**. Full details can be found within the main body of this document.

The sky coverage of each element of the Version 2.0 SWIRE data is illustrated in Figures 1-20. The user should be aware that there exist sources in each of the three catalogs with no coverage in one or both of the other catalogs, **thus a null-value in a given band may indicate lack of coverage rather than non-detection**. A boolean coverage flag is provided to indicate the presence of data coverage.

The user is also cautioned that there is incomplete optical coverage of the Spitzer areas, so **a non-detection in the optical more than likely means lack of optical imaging**. Furthermore there are gaps between the chips of the optical imaging arrays, so **optically-blank Spitzer sources can occur due to lack of optical coverage even within the boundaries of the optically imaged area.**

The IRAC+24μm catalog is a 3.6μm-selected catalog with a requirement that a detection also exists at 4.5μm, and with SNR thresholds imposed on each band. These requirements were imposed to ensure high levels of source reliability. Therefore **the catalog does not contain single band sources, nor sources not detected above the SNR thresholds at both 3.6μm and 4.5μm**.

The IRAC+24μm catalog **is not a flux-limited catalog**, because the varying coverage levels across the field have been taken into account when deriving the SNR-based thresholds for source inclusion. We chose to make the individual MIPS catalogs flux-limited, because coverage is very even for MIPS.

Bright stars may be missing or have distorted flux measurement in the IRAC-24μm Catalog owing to detector saturation and source extractor limitations.

The IRAC and MIPS 24μm source extraction has been done with aperture photometry. This can result in source confusion where the flux of one source can erroneously contaminate the measurement of a nearby source. The problem is worst at 24μm due to the large PSF size. **Photometry of close multiple objects**

should be carefully investigated on the images, especially at 24μm.

The processor which merges detections across the IRAC+24μm bands has limited performance in confused regions when the source density approaches the PSF. **There may remain some erroneous or failed merges within the catalog**, despite exhaustive efforts to remove them.

Optical identifications to Spitzer sources have been optimized for completeness rather than reliability, therefore **optical cross-identifications should be treated carefully, especially at faint magnitudes for source separations >0.5″.**

Cosmic rays have been exhaustively identified and removed from the SWIRE Spitzer DR2 images, however there may exist some unidentified CRs lying preferentially on top of real sources where it is most difficult to identify them. **Unusual source colors may indicate cosmic ray contamination and the user is urged to view images of such sources**. Cosmic ray contamination is worst in the 5.8μm band.

The SWIRE image processing for IRAC has been undertaken in "tiles" for computational reasons, and duplicates of sources lying along the overlapping tile edges may exist in the primary database. **It is possible that some duplicates have failed our duplicate rejection algorithm, resulting in a source appearing twice in the catalog.**

None of the Spitzer images have accurate absolute backgrounds. The Spitzer instruments are limited in their ability to measure the true celestial background, which at these wavelengths continuously varies due to the changing relative geometry of Spitzer, the sun, and the zodiacal cloud. SWIRE is designed to detect compact sources, and the manner in which the data was processed reflects this.

Image products for 160μm band are now known to have 5″ systematic astrometry errors in the cross-scan direction. The celestial coordinates in the 160μm catalogs have been corrected for this error.

In Section 2 we list the differences between this data release and the one preceding it. In Section 3 we describe the SWIRE Legacy Survey fields. In Section 4 we describe the release schedule. Section 5 details the observations while Section 6 details the data reduction. In Section 7 we provide full details of the data products. Section 8 presents an analysis of the quality of the data products, including an assessment of the reliability and completeness levels of the catalogs. **Finally Section 9 provides further details on caveats and cautions that users need to take into account when using these data products.**

2. Changes from Data Release 1

The Release 2 data includes a full re-release of all data products in Release 1. The new data entirely supplants the previous release. Users should now only use the new data products. Below we detail the primary differences between the new and old data. Most of these are treated in greater detail in the section on Data Processing.

2.1. Image Processing

- *Changes in Initial SSC BCD Products* — All IRAC data and the MIPS 70 and 160μm data were processed using the S11 data pipelines. Most relevant for IRAC is a considerably lower photometric noise from the flat-fields due to the SSC switching to high accuracy flats. MIPS processing is now

based on the "filtered BCDs" for both 70 and 160 microns.

- *Additional Artifact Mitigation in IRAC* — In this release, the muxbleed and banding artifacts have had a correction applied to them. In Release 1 these artifacts were masked but not corrected.

- *Change in IRAC Background Handling* — In Release 1, IRAC backgrounds were forced, on an individual frame-basis, to match a COBE-based model which generally predicted a gradient in the zodiacal background across the field. In Release 2, the data are forced to match the same model, but all of the data are set equal to the value predicted at the field center.

- *Changes in IRAC Flux Calibration* — The underlying calibration of the IRAC data has been adjusted by the SSC. The overall flux calibration has changed at the level of a few percent.

- *IRAC Array-Position Dependent Corrections* — A position dependent correction has been applied to the IRAC data in order to correct for systematic flux errors introduced by IRAC flat-fielding using the zodiacal background.

- *Correction of Outlier-Rejection Induced Flux Errors* — Problems with the coadder outlier rejection interacting with our low IRAC coverage levels led to a systematic underestimate in IRAC fluxes of order 15% for objects lying between 10 and 30σ. This has been corrected.

- *Changes in IRAC Pointing Refinement* — Use of the SSC-generated refined pointing at 5.6 and 8μm was discontinued.

- *Long-Term Latent Mitigation* — Slow-decay image latents present at 3.6μm have been corrected.

- *Additional Image Data Products* — Pseudo-truecolor images made from IRAC 3.6, 4.5, and 8μm data are provided.

- *Filling of MIPS Gap in ELAIS N1 Map* – The Release 2 MIPS maps include additional observations taken in late July 2004. These fill in a gap in the Release 1 maps caused by an observatory standby event.

2.2. Catalog Generation

- *Lower Flux Limits* — the catalogs now extend to lower flux levels.

- *Data Coverage Flags* — additional flags in the catalogs now indicate if non-detections are due to a lack of data.

- *Additional Flux Measurements* — IRAC data now includes five different aperture fluxes, extended source measurements, and a flag indicating which flux measurement is likely to be the most representative of the "total" flux. MIPS 24μm processing includes four aperture fluxes as well as extended source measurements.

- *MIPS Color Corrections Included* — The MIPS extractions have been adjusted upwards by a few percent to quote the flux densities for a $\nu F_\nu = $ constant spectrum.

- *New Point Source Extraction at 70 and 160 microns* — Source extraction for Release 2 for the MIPS Germanium bands now uses the SSC's APEX point source extractor.

3.   The SWIRE Survey

The Spitzer Wide-area InfraRed Extragalactic survey (SWIRE), the largest Spitzer Legacy program, is a wide-area, imaging survey to trace the evolution of dusty, star-forming galaxies, evolved stellar populations, and AGN as a function of environment, from redshifts z∼3 to the current epoch. SWIRE surveys 6 high-latitude fields, totaling ∼ 50 sq. deg. in all 7 SIRTF bands: 3.6, 4.5, 5.8, and 8μm with IRAC and 24, 70, and 160μm with MIPS (Lonsdale et al. 2003). The SWIRE Legacy Extragalactic Source Catalogs will eventually contain in excess of 2 million IR-selected galaxies, from those dominated by the light of stellar populations detected primarily by IRAC, to starbursts, ultra-luminous infrared galaxies (ULIRGs: log $L_{FIR} > 10^{12}$ $L_{\odot}$) and AGN detected also by MIPS. The key scientific goals of SWIRE are to determine: (1) the evolution of actively star-forming and passively evolving galaxies to determine the history of galaxy formation in the context of cosmic structure formation; (2) the evolution of the spatial distribution and clustering of evolved galaxies, starbursts and AGN in the key redshift range, 0.5<z<1.5, when the sharp decline in star formation activity has occurred; (3) the evolutionary relationship between "normal galaxies" and AGN, and the contribution of AGN accretion energy *vs.* stellar nucleosynthesis to the cosmic backgrounds. The large area of SWIRE is important to establish statistically significant population samples over enough volume cells that we can resolve the star formation history as a function of epoch and environment, *i.e.* in the context of structure formation. The large volume is also optimized for finding rare objects.

The SWIRE fields are becoming the next generation of *large* "Cosmic Windows" into the extragalactic sky. They have been uniquely selected to minimize Galactic cirrus emission over large scales (which dominates the far-infrared non-cosmological backgrounds), while also minimizing background emission from the zodiacal cloud, which dominates at mid-infrared wavelengths. As such, they are the best locations for multi-degree areal surveys where Spitzer can achieve observations of great depth efficiently. GALEX is observing them as part of its deep survey. SWIRE includes ∼9 sq deg of the unique large-area XMM-LSS hard X-ray imaging survey, and is partly covered by the UKIDSS deep J & K survey. An extensive optical/near-IR imaging program is underway from the ground. Other SWIRE fields include the well-studied Lockman Hole and a large area surrounding the deeper GOODS and GEMS survey in the CDF-S.

A preview of the SWIRE galaxy populations has been published by Lonsdale *et al.* (2004) and an investigation of the correlation function by Oliver *et al.* (2004). Rowan-Robinson *et al.* (2004) present a detailed SED (spectral energy distribution) and photometric redshift analysis of SWIRE populations, while Hatziminaoglou *et al.* (2004) identify and investigate Sloan Digital Sky Survey (SDSS) QSOs in the field. Franceschini *et al.* (2004) analyze SWIRE-Xray identifications from the deep Chandra image in N1. The first SWIRE number counts are presented by Shupe *et al.* (2005) and Surace *et al.* (2005). Polletta *et al.* (2005) present a detailed SED- and color-based analysis of the SWIRE galaxy populations and Davoodi *et al.* (2005) investigate a cluster analysis approach to SWIRE population characterization.

3.1.   The ELAIS-N1 Field

The first SWIRE field to be observed by Spitzer was the European Large Area ISO Survey (ELAIS) field N1, which is one of 5 fields observed by ISO as part of the 11 square degree ISO ELAIS survey. Details of the final band-merged ELAIS Catalog and of the ISO data-processing are given in Rowan-Robinson et al (2004). A 20-cm radio survey was carried out in this area by Ciliegi et al (1999) and Manners et al (2003) have reported Chandra observations of the central region of N1. Optical associations of ELAIS sources using the INT WFS survey were described by Gonzalez-Solares et al (2004), and spectroscopic follow-up by

Perez-Fournon et al (2004, in preparation) and Serjeant et al (2004). Part of N1 was surveyed in J and K by Vaisanen et al (2002). This region also contains a deep HST-ACS pointing. It also contains a deep pointing of some 50 square arcminutes with IRAC and MIPS, taken as part of the extragalactic First Look Survey program (see Figure 1).
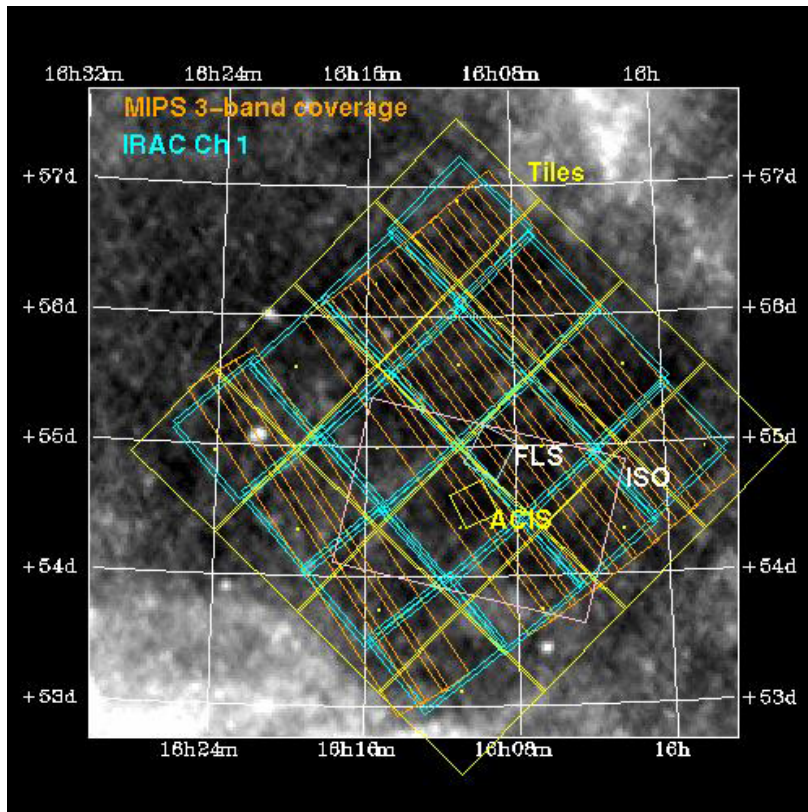

Fig. 1.— SWIRE ELAIS N1 field, as observed by SWIRE. Shown in orange are the MIPS scan legs, in blue the IRAC AORs (astronomical observing requests). Yellow and white show some of the additional surveys located within the SWIRE field. Also in yellow is the "tile" scheme used by SWIRE for data delivery, and shown more clearly in Figure 4. The fields are shown overlaid on a 100μm IRAS-ISSA plate.

3.2. The ELAIS-N2 Field

Another part of the ELAIS survey, this field is relatively near the first, and is somewhat smaller.

3.3. The XMM-LSS Field

SWIRE observations of the XMM-LSS were performed in July 2004, covering a 9.1 deg^2 area. Despite the somewhat higher IR background of the region, the extensive multi-wavelength coverage of the field makes its especially relevant for environmental studies. In addition to the XMM observations the field (or some fraction of it) is covered by VLA, GALEX, UKIDSS and CFHTLS observation as well by the Vimos very

Deep Survey (see Pierre et al 2004, for a general description of these surveys).

XMM source lists have been issued thanks to a dedicated wavelet-based based pipeline providing enhanced spatial resolution, hence well controlled point-like/extended source selection effects (Pacaud et. al. 2005) which is critical for galaxy cluster science. Spectroscopic identification of more than 50 clusters out to a redshift of 1 is completed and the resulting cluster catalogue will be released together with general multi-band source lists by the end of 2005. X-ray information, as well as associated weak lensing analysis of the field will provide important information on cluster properties, especially mass estimates, which are fundamental parameters for further environmental studies. The most important characteristic of the cluster sample is the presence of a large fraction of low-mass galaxy groups up to z~0.5, providing a cluster density of $15/\text{deg}^2$, the highest to date over a single area (these findings are in accordance with the LCDM cosmology, Pierre at 2005). With a density over $200/\text{deg}^2$ down to a flux limit of 5E-15 erg/s/cm^2 in the [0.5-2] keV band, the X-ray AGN population is well sampled. Along with the SWIRE data, this allows the identification of a number of obscured objects and the study of their location within the overall large scale cosmic network.

By the final release of the SWIRE data (mid-2006), CFHTLS optical identifications for all SWIRE sources will be provided: u,g,r,i,z magnitudes as available, and an indication of whether they are pointlike in the optical.

3.4. The Lockman Hole Field

SWIRE observations of the"Lockman Hole" field were carried out in April/May 2004 over a region of 11 square degrees making Lockman SWIRE's largest survey field. This field, originally noted by Lockman, Jahoda, and McCammon (1986, ApJ, 302, 432) as a minimum in the Galactic HI distribution with $N_H I \sim 4.5x10^{19}$ cm$^-$2, is possibly the largest-area, lowest-IR-background ($< S_1 00\mu m > \sim 0.4$ MJy/sr) field in the sky (Oliver et al. 2005, in prep), and it has been the target for numerous extragalactic surveys in many wavebands. A deep 2MASS survey with $J < 17.8$, $H < 16.5$, $K_S < 16.0$ (Beichman et al. 2003, AJ, 125, 2521) covers the entire SWIRE field. Other, smaller surveys of particular interest to SWIRE are ISO surveys at $7\mu m$ (Taniguchi et al. 1997, AA, 328, L9), $14.3\mu m$ (Fadda et al. 2004, AA, 427, 23), $95\mu m$ (Rodighiero et al. 2005, MNRAS, 357, 449) and $175\mu m$ (Kawara et al. 1998, AA, 336, L9); radio surveys at 6cm (Ciliegi et al. 2003, AA, 398, 901) and 20cm (de Ruiter et al. 1997, AA, 319, 7); millimeter/submillimeter surveys (Bolocam 1mm Survey: Laurent et al. 2005, ApJ, 623, 742; SCUBA 8mJy Survey: Scott et al. 2002, MNRAS, 331, 817; SCUBA HAlf Degree Extragalactic Survey - SHADES: Dunlop 2005, ASSL, 329, 121); and x-ray surveys with ROSAT (Hasinger et al. 1998, AA, 329, 482), ASCA (Ishiaki et al. 2001, PASJ, 53, 445), XMM-Newton (Hasinger et al. 2001, AA, 365, L45) and Chandra (Yang et al. 2003, ApJ, 585, 85:Lockman NW). The "Lockman-East" field with XMM-Newton and SHADES observations is the site of a GTO Deep Survey of area $\sim 25' \times 2$ deg.

In addition to the Spitzer Observations in Lockman, the SWIRE Team has carried out a single-pointing deep VLA survey with 20cm sensitivity $\sim 3\mu$Jy (Owen et al. 2005, in prep) and a 0.6 deg^2, 70ks/pointing Chandra survey (Polletta et al. 2005, in prep.), both centered at 10h46m +59d01m. Deep imaging has been carried out over 7 sq deg of the Lockman Field with the KPNO Mosaic Camera on the 4-m Mayall Telescope to approximate depths of g$' \sim 25.7$, r$' \sim 24.7$, i$' \sim 24$ (Siana et al. 2005, in prep). The Chandra/Radio field served as SWIRE's validation field so that IRAC observations are about 1.4 times deeper and MIPS observations about 1.2 times deeper over a 0.5 deg^2 area. U-band imaging is also available over the Chandra/Radio field to U 24. INT/WFC camera r$'$ observations cover the southern portion of the field to r$' \sim 23.8$.

4. Phased Release of Data

The data included in this release are summarized in Tables 1-6. Full details of these products are provided in Section 6. Users should note that this data release has been phased over the summer of 2005. Release dates are:

June 22, 2005

- IRAC and MIPS mosaicked images for ELAIS-N1, ELAIS-N2, Lockman Hole, XMM-LSS

- 3-color IRAC images for ELAIS-N1, ELAIS-N2, Lockman Hole, XMM-LSS

July 25, 2005

- Optical ancillary images for ELAIS-N1 and ELAIS-N2 available

- Optical-IRAC-MIPS24 bandmerged catalog for ELAIS-N1 available through the SSC and IRSA-Gator

August 20, 2005

- Optical-IRAC-MIPS24 bandmerged catalog for ELAIS-N2 and XMM-LSS available through the SSC.

The release of the Lockman Hole catalogs and optical image daata may be delayed until October 2005 to allow for filling of the embargoed region and additional processing. The advanced data products may be acquired from the Spitzer Science Center[2]. Many users may wish to consider accessing the actual catalogs via the IRSA "Gator" service[3]. This is a web-based catalog query service that allows sophisticated selection of subsets of the data.

5. Observations

5.1. Spitzer Data

The SWIRE Data Release 2 includes only data from the ELAIS-N1, ELAIS-N2, Lockman Hole, and XMM-LSS regions. The next data release, expected in Fall '05 will contain the two final fields, the Chandra Deep Field South and ELAIS-S1. It consists of a total of 182 Astronomical Observation Requests (AORs), the basic unit of Spitzer observations. Due to the sheer number of AORs, we do not give their request numbers here. The actual AORs can be retrieved via SPOT, and the frame-level data itself can be retrieved via Leopard[4]. The program IDs are given in Table 2. These uniquely identify each SWIRE field in the Spitzer database.

---

[2]http://ssc.spitzer.caltech.edu/legacy/

[3]http://irsa.ipac.caltech.edu/applications/Gator/

[4]http://ssc.spitzer.caltech.edu/propkit/spot/

SWIRE Data Release 2 Catalog Data				
Field	Instruments	λ Coverage	# Entries	Volume (MB)
ELAIS-N1	INT/WFC,IRAC,MIPS	0.36—24	282711	597
	MIPS	24	?	?
	MIPS	70	?	?
	MIPS	160	?	?
ELAIS-N2	INT/WFC,IRAC,MIPS	0.36—24	126056	266
	MIPS	24	?	?
	MIPS	70	?	?
	MIPS	160	?	?
Lockman Hole	KPNO,IRAC,MIPS	0.36—24	301061	609
	MIPS	24	?	?
	MIPS	70	?	?
	MIPS	160	?	?
XMM-LSS	IRAC,MIPS	3.6—24	250733	399
	MIPS	24	?	?
	MIPS	70	?	?
	MIPS	160	?	?

Table 1: Summary of catalog data included in the SWIRE Data Release 2. A "?" indicates that the given catalog has not yet been delivered.

5.1.1. IRAC

Each field is mapped by IRAC with a large grid of AORs. The grid spacing was $280''$, which is 90% of the detector width. At each grid point two 30-second images were taken. Between frames a small cycling dither pattern was employed. The AORs themselves were arranged on a 4×4 grid. The entire grid was repeated in two epochs. The two different epochs were offset by 1/2-array width, and typically follow one another with a temporal spacing of 2.5 hours. Thus, for any point on the sky there are a minimum of four independent sightings (images), and these sightings occur on widely spaced parts of the detector array in order to minimize instrumental signatures arising in the detectors. The entire survey has a minimum depth of four coverages, equal to 120 seconds of exposure time. In some areas this can be as high as sixteen coverages, or 480 seconds. Because the 3.6 & 5.8μm detectors share a different field of view than the 4.5 and 8μm detectors, the coverage is not the same between bands. There are a total of 92,743 images in Data Release 2. Figure 2 shows a single AOR, and the same AOR overlaid with the second epoch of observation.

Field	PID	Dates	
		IRAC	MIPS
ELAIS-N1	185	01/14/04—01/20/04	01/21/04—01/28/04, 07/29/04
ELAIS-N2	183	07/05/04—07/06/04	07/08/04—07/11/04
Lockman Hole	142	04/24/04—04/30/04	05/04/04—05/10/04
XMM-LSS	181	07/23/04—07/28/04	07/30/04—08/05/04

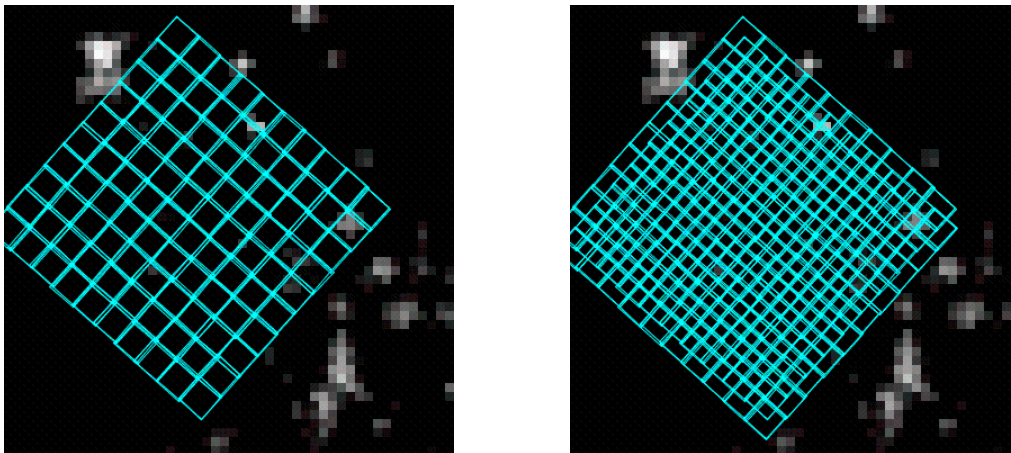Table 2: Summary of Program IDs and observation dates for the Spitzer data.

Fig. 2.— (Left) a single IRAC AOR, overlayed on a 100μm IRAS-ISSA image. There are two dithered pointings at each map position. (Right) The second epoch of IRAC overlayed on the first. The second epoch is offset by 1/2 the array size in both directions.

5.1.2. MIPS

The Scan Map mode was used with medium scan rate, and a leg-to-leg spacing of 148 arcseconds. The AORs were arranged into two coverages. The second coverage AORs were offset by 150 arcseconds in the cross-scan direction, and adjacent AORs were overlapped by 239 arcseconds to ensure overlap of the good half of the 70μm array. With this observation layout, the nominal coverage per point is 40 Basic Calibrated Data (BCD) images in the MIPS 24μm band. In the 70μm band, slightly less than half the array is usable, yielding nominally 20 BCDs per sky position. In the 160μm band, 4 images per point are obtained. The exposure time per BCD is 4 seconds, giving a total integration time per point of 160s, 80s, 16s for the 24, 70 and 160μm bands respectively. Due to the rotation of the Spitzer field of view over the course of the SWIRE observations, there are overlap regions between scan legs that have slightly higher coverage.

5.1.3. Missing Data

There are several instances of missing data in the SWIRE data products. The first example of these is intentional. Specifically, the Lockman Hole field overlaps with a Spitzer Guaranteed Time Observer (GTO), PID 81, which images a smaller region of this field more deeply than SWIRE. The entire AOR which overlaps this field is currently embargoed by the SSC, and will be included in a future data release. This issue affects both the IRAC and MIPS data.

Additionally, there are subregions typically $5\times10'$ in size internal to the 3.6μm Lockman Hole data and all IRAC bands of the XMM-LSS data which have been deliberately blanked as a result of missing data. The underlying raw data in these regions were damaged upon transmission to the ground, and as a result were never processed by the SSC into BCD data. Data coverage was either zero or too low for reliable outlier rejection as a result, and so the regions have been blanked to ensure that they are recognized as unusable. SWIRE will attempt to recover these data for future releases.

5.1.4. ELAIS-N1 MIPS Anomaly

Spitzer went into standby mode on 2004 January 25, leading to the loss of five of the SWIRE AORs (numbers 22-26 out of the sequence of 32). The last six AORs were taken after the observatory was restored to operations. However, the telescope warmed up slightly to 6 K during the standby mode, which affected the DC level of the MIPS data in the first few AORs after recovery. The lost AORs were re-observed July 28-29, 2004, and have been included in this release.

SWIRE ELAIS-N1 Data Release 2 Image Data					
Instrument	λ (μm)	# primary images	# ancillary images	Total Volume (MB)	Area ($\square^\circ$)
INT/WFC	0.36	15	0	6750	6.5
INT/WFC	0.52	15	0	6750	6.5
INT/WFC	0.67	15	0	6750	6.5
INT/WFC	0.79	15	0	6750	6.5
INT/WFC	0.91	15	0	6750	6.5
IRAC	3.6	16	48	6300	9.3
IRAC	4.5	16	48	6300	9.3
IRAC	5.8	16	48	6300	9.3
IRAC	8.0	16	48	6300	9.3
MIPS	24	1	1	796	8.5
MIPS	70	1	2	192	8.5
MIPS	160	2	1	30	8.5

Table 3: Summary of image data included in the ELAIS-N1 SWIRE Data Release 2. Note that the actual areal coverage of the Catalog is somewhat smaller - see Section 7.3.1.

SWIRE ELAIS-N2 Data Release 2 Image Data					
Instrument	λ (μm)	# primary images	# ancillary images	Total Volume (MB)	Area ($\square^\circ$)
INT/WFC	0.36	6	0	3100	5.4
INT/WFC	0.52	6	0	3100	5.4
INT/WFC	0.67	6	0	3100	5.4
INT/WFC	0.79	6	0	3100	5.4
INT/WFC	0.91	6	0	3100	5.4
IRAC	3.6	6	18	2772	4.2
IRAC	4.5	6	18	2772	4.2
IRAC	5.8	6	18	2772	4.2
IRAC	8.0	6	18	2772	4.2
MIPS	24	1	1	448	5.8
MIPS	70	1	2	93	5.7
MIPS	160	2	1	23	5.7

Table 4: Summary of image data included in the ELAIS-N2 SWIRE Data Release 2. Note that the actual areal coverage of the Catalog is somewhat smaller - see Section 7.3.1.

SWIRE Lockman Hole Data Release 2 Image Data					
Instrument	λ (μm)	# primary images	# ancillary images	Total Volume (MB)	Area ($\Box^\circ$)
IRAC	3.6	20	60	7120	10.5
IRAC	4.5	20	60	7120	10.5
IRAC	5.8	20	60	7120	10.5
IRAC	8.0	20	60	7120	10.5
MIPS	24	20	20	448	11.9
MIPS	70	1	2	269	12.4
MIPS	160	2	1	66	12.1

Table 5: Summary of image data included in the Lockman Hole SWIRE Data Release 2. Note that the actual areal coverage of the Catalog is somewhat smaller - see Section 7.3.1.

SWIRE XMM-LSS Data Release 2 Image Data					
Instrument	λ (μm)	# primary images	# ancillary images	Total Volume (MB)	Area ($\Box^\circ$)
IRAC	3.6	16	48	5376	9.1
IRAC	4.5	16	48	5376	9.1
IRAC	5.8	16	48	5376	9.1
IRAC	8.0	16	48	5376	9.1
MIPS	24	1	1	940	10.6
MIPS	70	1	2	156	10.4
MIPS	160	2	1	39	10.3

Table 6: Summary of image data included in the XMM-LSS SWIRE Data Release 2. Note that the actual areal coverage of the Catalog is somewhat smaller - see Section 7.3.1.
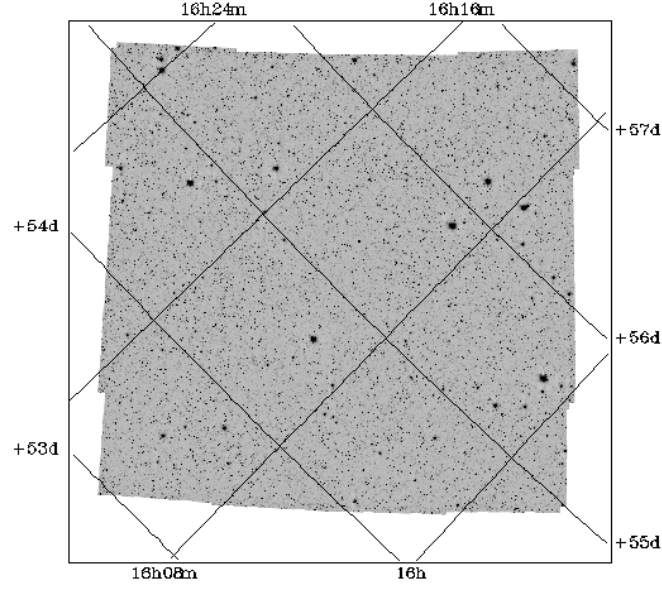
Fig. 3.— SWIRE ELAIS N1 field at 3.6μm, as observed by SWIRE.
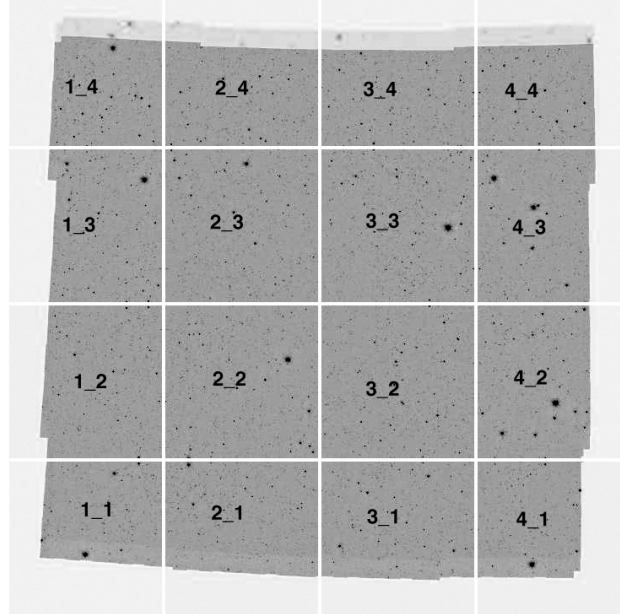
Fig. 4.— SWIRE "tile" system, overlaid on the IRAC data.
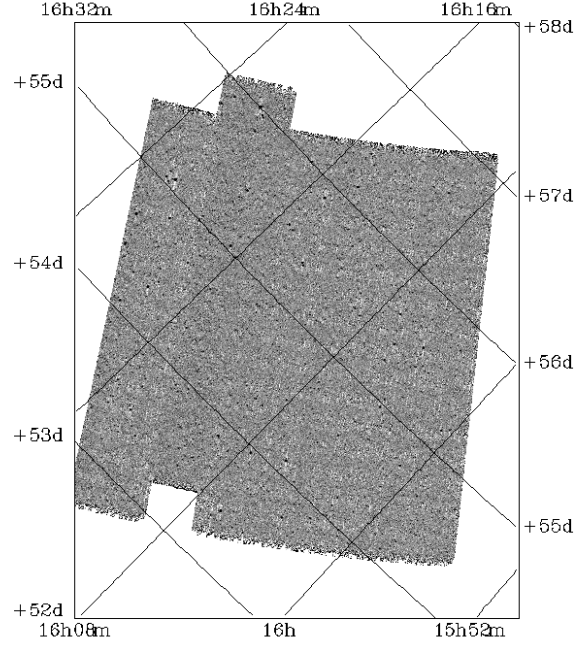
Fig. 5.— SWIRE ELAIS N1 field at 70μm, as observed by SWIRE. The offset is a result of that strip of data being observed six months later than the rest of the field. This resulted in a 180° rotation of the detector, and as a result the "spillover" at the end of the MIPS scan leg is on the other side of the field.
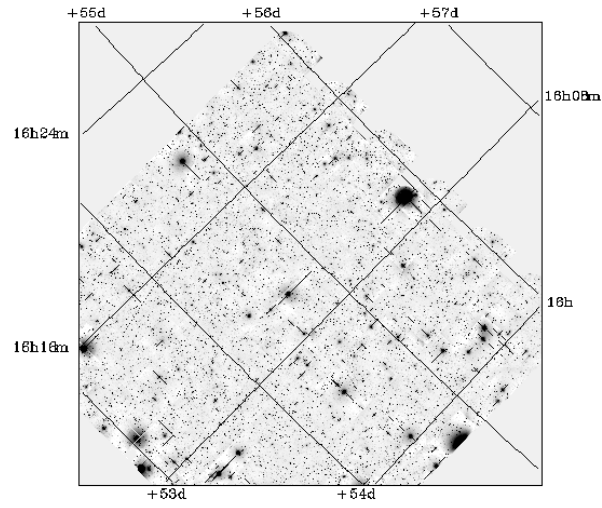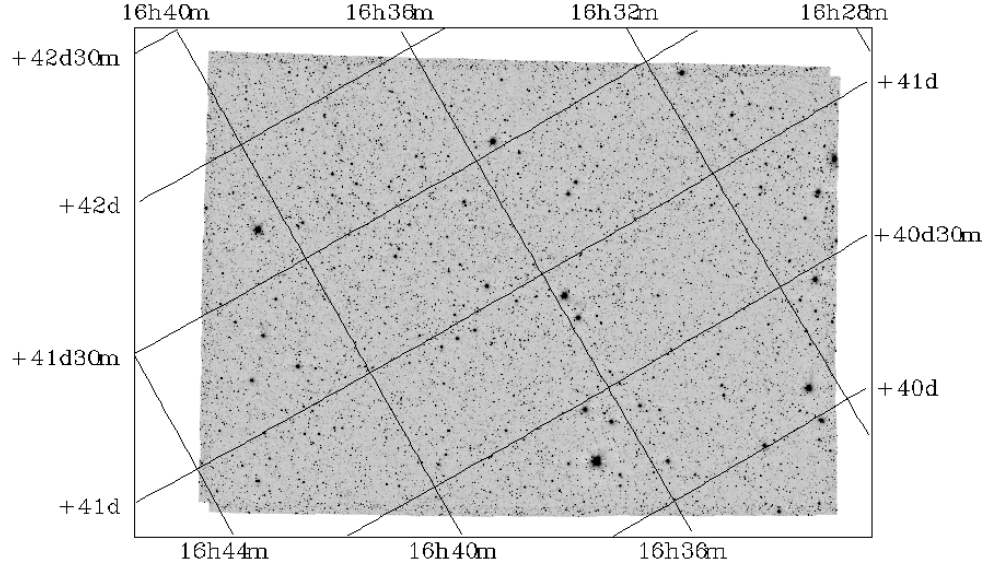

Fig. 6.— ELAIS-N1 field r-band data.

Fig. 7.— SWIRE ELAIS-N2 field at 3.6μm, as observed by SWIRE.
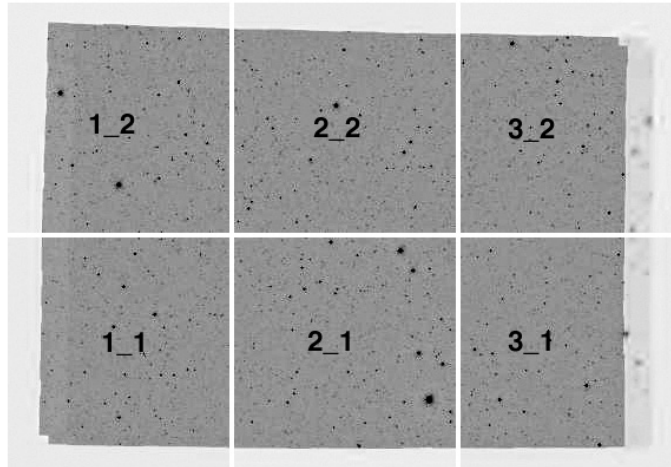
Fig. 8.— IRAC SWIRE "tile" system for ELAIS-N2.
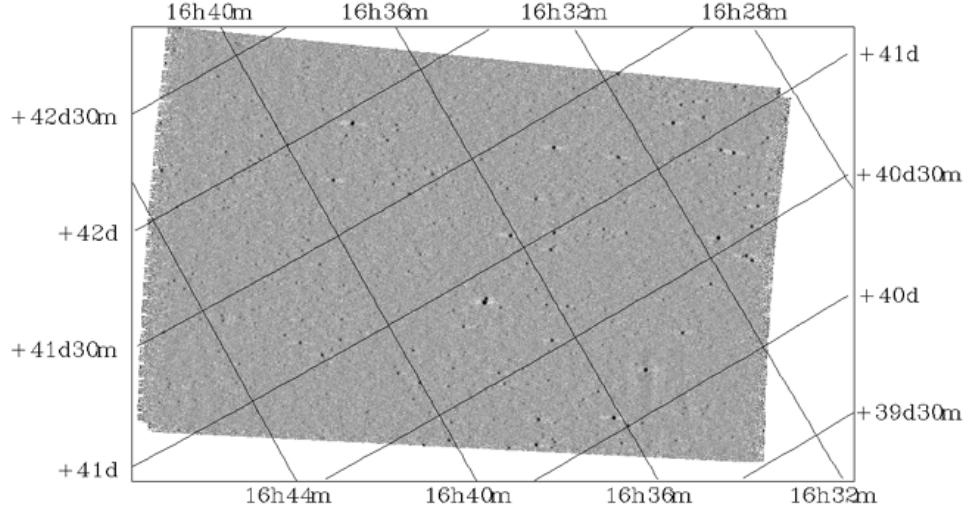
Fig. 9.— SWIRE ELAIS-N2 field at 70μm, as observed by SWIRE.
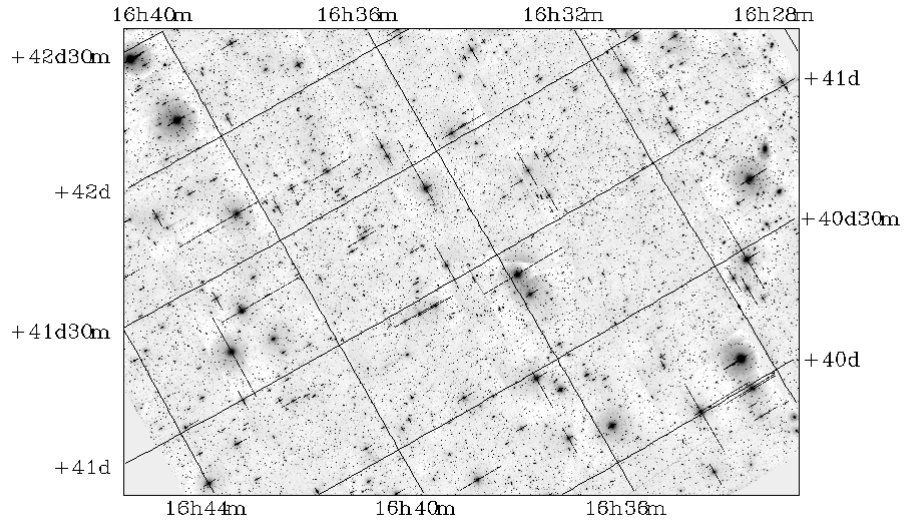
Fig. 10.— ELAIS-N2 field r-band data. All of the ELAIS-N2 field has matching optical data.
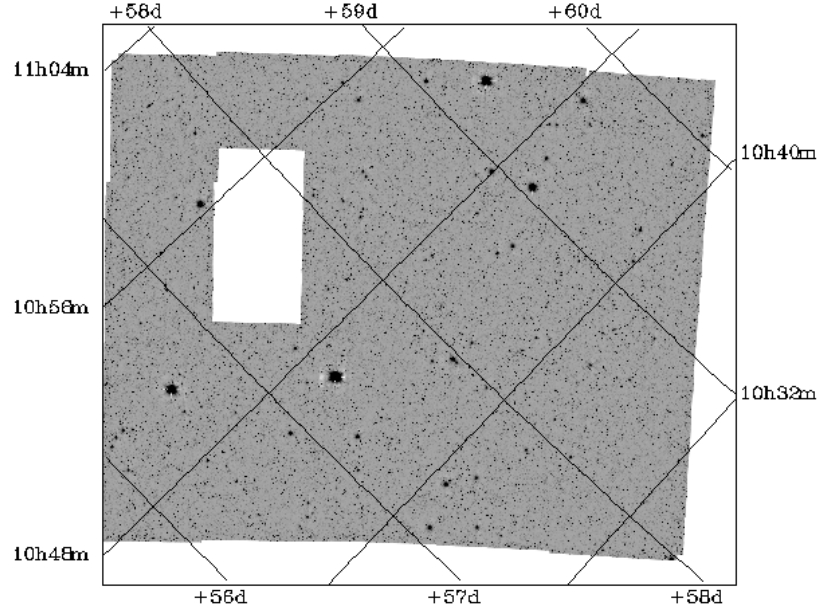
Fig. 11.— SWIRE Lockman Hole field at 3.6μm, as observed by SWIRE. The SWIRE data is partially embargoed in this field as a result of overlap with proprietary GTO data, resulting in the data gap interior to the field. Future data releases will include this data.
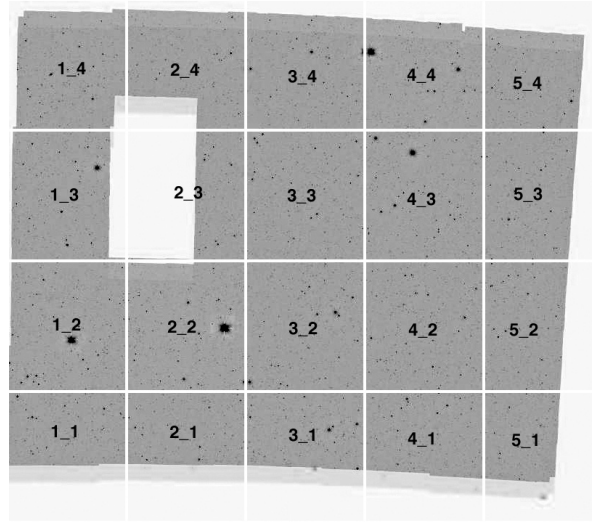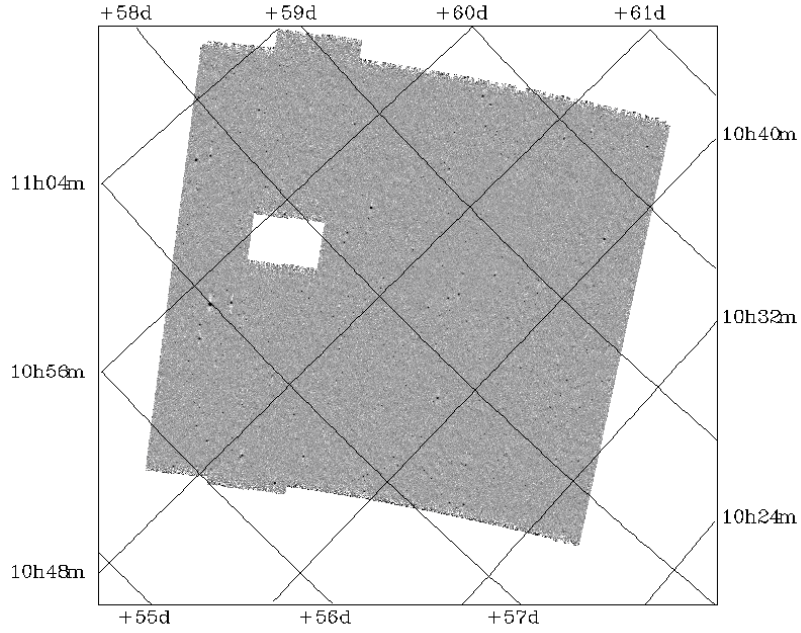

Fig. 12.— IRAC SWIRE "tile" system.

Fig. 13.— SWIRE Lockman Hole field at 70μm, as observed by SWIRE. The SWIRE data is partially embargoed in this field as a result of overlap with proprietary GTO data, resulting in the data gap interior to the field. Future data releases will include this data.
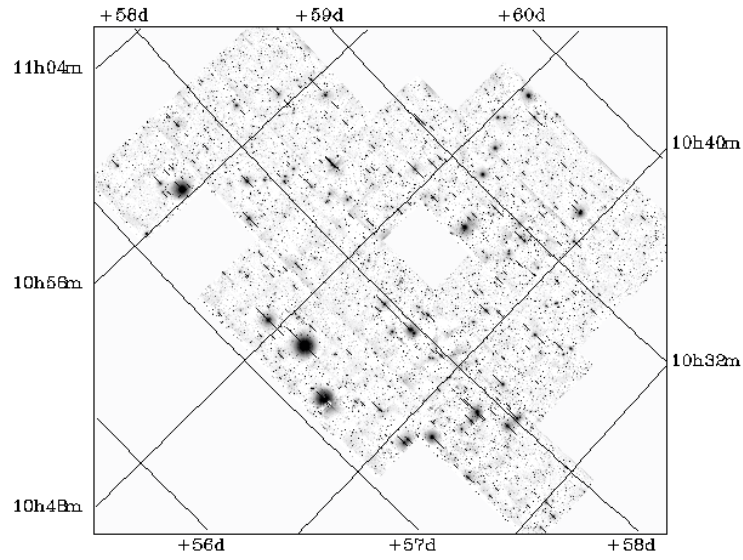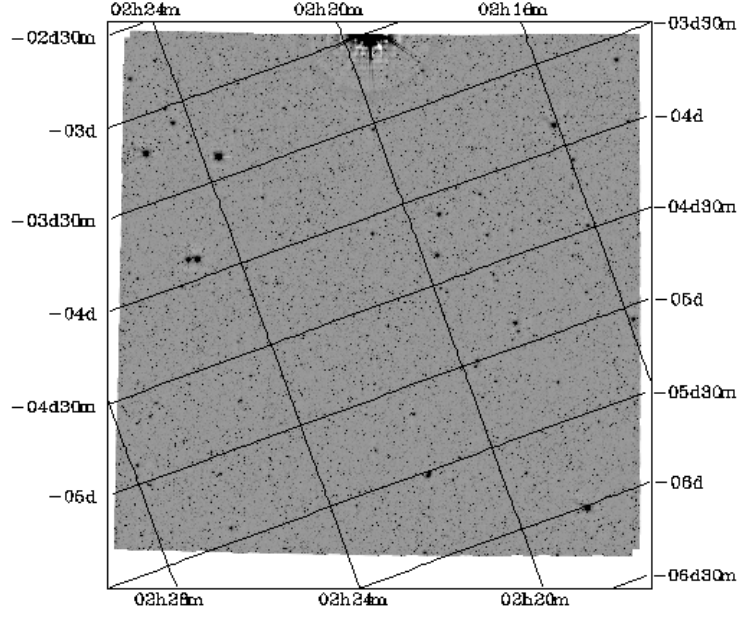

Fig. 14.— Lockman Hole r-band data.

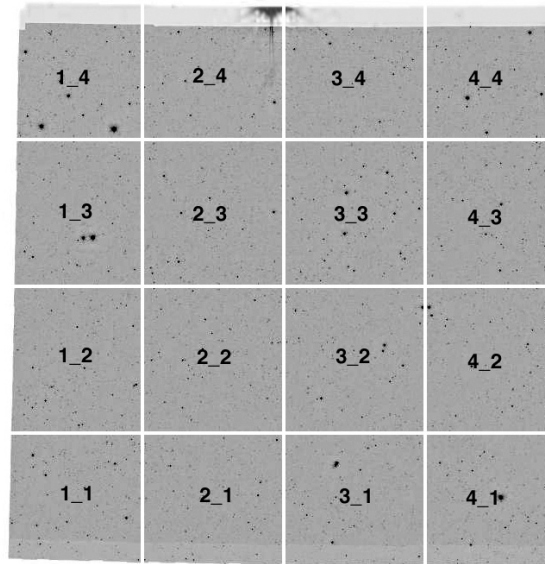Fig. 15.— SWIRE XMM-LSS field at 3.6μm, as observed by SWIRE.
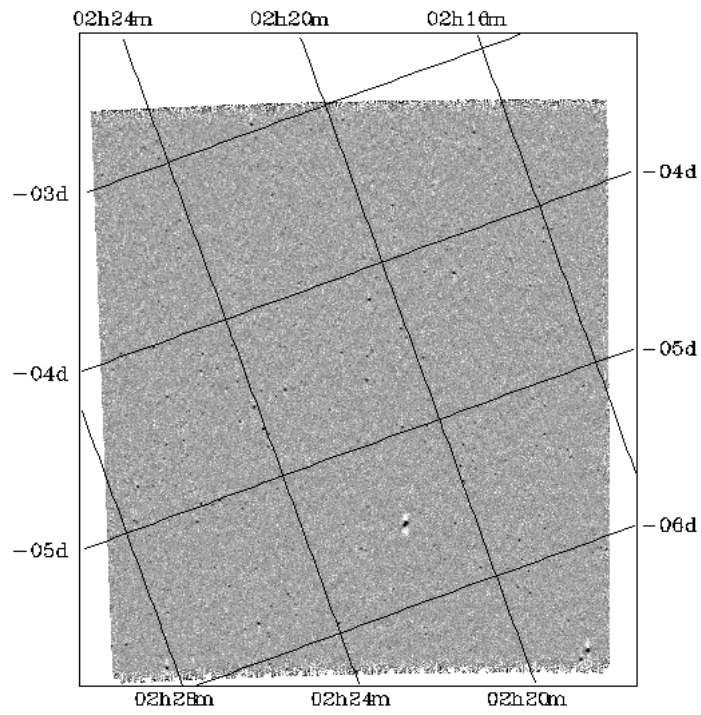

Fig. 16.— IRAC SWIRE "tile" system.

Fig. 17.— SWIRE XMM-LSS field at 70μm, as observed by SWIRE.

5.2. Optical Data

5.2.1. ELAIS-N1

The Wide Field Survey has been carried out using the Wide Field Camera (WFC) on the 2.5m Isaac Newton Telescope (INT) on the Observatorio del Roque de Los Muchachos (La Palma, Spain). The WFC is formed by four 4k x 2k CCDs. The arrays have 13.5 micron pixels corresponding to 0.33″/pixel at the telescope prime focus and each one covers an area on sky of 22.8 x 11.4 arcmin. The total sky coverage per exposure for the array is therefore 0.29 square degrees. Gaps between detectors are typically 20″. Chip 3 is slightly vignetted in one corner. Optical observations are carried out allowing for a 10% overlap between adjacent pointings for photometric purposes. Typical seeing is about 1.2″.

The survey consists of single 600s exposures in five bands: U, g′, r′, i′ and Z to magnitude limits of: 23.4, 24.9, 24.0, 23.2, 21.9 respectively (Vega, 5σ for a point-like object), i.e., about 1 magnitude deeper than the Sloan Digital Sky Survey. The filter bandpasses are given in Table 7. More details including filter responses, photometric information, etc. are available at the INT WFS web site[5].

Filter	Central Wavelength	FWHM	ab_conv
U_WFC	3624.3	600.0	0.7887
g_WFC	4885.3	1220.0	-0.0888
r_WFC	6240.0	1340.0	0.1571
i_WFC	7696.4	1515.0	0.3945
Z_WFC	9120.7	1470.0	0.5674

Table 7: Filter system for the Wide Field Survey. ab_conv is the factor required to convert the Catalog magnitudes to AB magnitudes: $AB = mag + ab\_conv$.

A total of 54 pointings were done in N1, covering a total area of 9 square degrees. However, not all of the WFS data overlaps the Spitzer data. Conversely, not all of the Spitzer data overlaps the optical data. Figure 18 illustrates the area covered by SWIRE with IRAC, and the overlapping area covered by the WFS.

5.2.2. ELAIS-N2

The ELAIS N2 data were acquired as part of the Wide Field Survey described above for ELAIS N1.

5.2.3. Lockman Hole

The optical data has been taken with the Mosaic-1 Camera[6] on the 4m Mayall Telescope at Kitt Peak National Observatory (KPNO). The Mosaic-1 Camera is a mosaic of 8 4k x 2k CCDs, with a pixel scale of 0.26 ″/pixel, and a 36x36 arcmin field of view. The gaps between the detectors are ∼13″ in the NS direction

---

[5]http://www.ast.cam.ac.uk/∼wfcsur/index.php

[6]http://www.noao.edu/kpno/mosaic/manual/

Fig. 18.— Location of the overlapping WFS optical data relative to the Spitzer data. All Spitzer -IRAC detections are shown in grey, while those that were also identified with WFS optical counterparts are shown in black. Approximately 70% of the SWIRE ELAIS N1 field is covered by optical data.
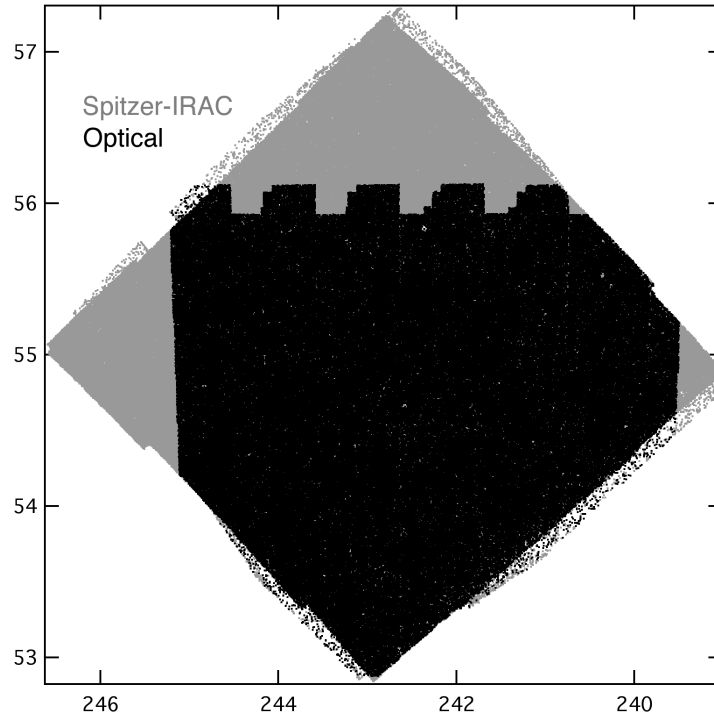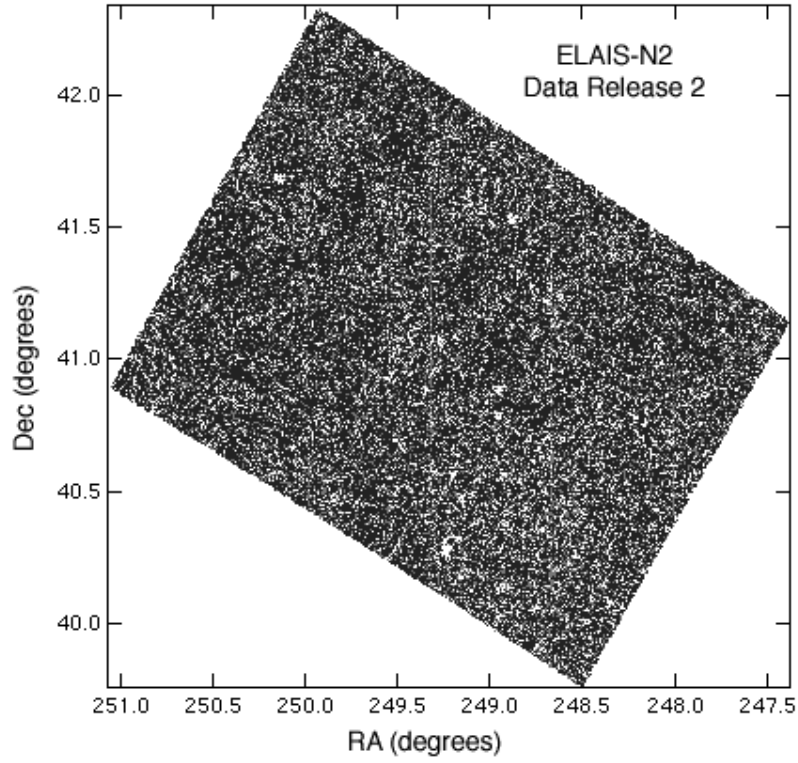
Fig. 19.— Location of the overlapping WFS optical data relative to the Spitzer data. All Spitzer -IRAC detections are shown in grey, while those that were also identified with WFS optical counterparts are shown in black. The entire ELAIS-N2 field has associated optical data.

and $\sim 9''$ in the EW direction. Adjacent pointings were typically separated by 32 arcminutes with a few exceptions due to Spitzer field rotations.

The survey consists of 5x360s exposures in g$'$, r$'$, & i$'$ dithered by $30''$ between exposures to cover the gaps between chips. The magnitude limits are approximately 25.1, 24.4, 23.7 respectively (Vega, 5σ point source) but vary significantly between pointings. 25 pointings were observed in these 3 primary filters (one field has only r$'$, and another has only r$'$ and i$'$) covering 7 deg^2. The four pointings which cover the SWIRE-Chandra field have deep U band imaging with 5x720s exposures to a magnitude limit of 24.1. The typical seeing was 1.2-1.3$''$.

Filter	KPNO Name	Central Wavelength	FWHM	ab_conv
U	k1001	3552	630.7	0.7887
g$'$	k1017	4750.6	1395.7	-0.0888
r$'$	k1018	6292.3	1475.2	0.1571
i$'$	k1019	7726.3	1539.9	0.3945

Table 8: Filter system for Mosaic-1 observations of the SWIRE Lockman Field. ab_conv is the factor required to convert the Catalog magnitudes to AB magnitudes: $AB = mag + ab\_conv$.

The images were reduced with the Cambridge Astronomical Survey Unit (CASU) pipeline. There is a scattered light effect causing a pupil ghost in the U and i$'$ bands. The amplitude of the scattered light image is small ($< 2\%$ of the background) and therefore there was no attempt to subtract it. Individual CCDs were stacked with data from the same CCDs and then extracted with a 3.1$''$ diameter aperture. For more information on the reduction and extraction routines, see the INT WFS website (above). Detailed information on the SWIRE Lockman ground-based campaign can be found in Siana et al. (2005, in prep).

5.2.4. XMM-LSS

The XMM-LSS region has been extensively survey by the CFHT Legacy Survey. However, this data is not publicly available and is not released by SWIRE. Members of the associated partners of the CFHTLS should contact them for data availability.

6. Data Processing

6.1. Spitzer Science Center Processing

IRAC data were processed by the Spitzer Science Center (SSC) during January-February 2005 using the SSC S11.4.0 software revision. The individual images have been linearized, flat-fielded, dark-subtracted and flux calibrated. Standard calibration products were used; specifically, contemporaneous darks and flats taken in the same campaign. The data are received by SWIRE fully reduced and flux-calibrated at the individual frame level. Details of the SSC IRAC pipeline can be found in the *IRAC Pipeline Description Document* and the *IRAC Data Handbook*[7].

The MIPS basic calibrated data products (BCDs) used for this data delivery were down-loaded from the public SSC data archive after being processed by the SSC pipeline software–version S10 for the 24μm data and version S11 for the MIPS-Ge data.. The BCD pipeline processing follows the algorithms derived by the MIPS Instrument Team which were designed on the basis of extensive pre-launch laboratory testing (Gordon et al. 2004). The details of the SSC MIPS-Ge BCD pipeline processing are provided in the FLS MIPS 70μm data paper (Frayer et al. 2005) and are described in the MIPS data handbook available on the web at the URL listed below. Details of the MIPS 24μm pipeline may also be found there.

6.2. SWIRE Processing

6.2.1. IRAC

Images

SWIRE processing of IRAC data begins with the SSC's Basic Calibrated Data (BCD). Individual images are received from the SSC. The data are ingested and registered into a database. Although we initially planned detailed quality checking of all incoming data, this was altered in response to the appearance of the actual flight data. An examination of initial validation data taken with the SWIRE data-taking scheme in the Lockman Hole region showed that the detector environments and associated detector responses were remarkably stable - anticipated transient problems, particularly due to radiation hits, did not significantly appear in the actual flight data. Indeed, the IRAC detectors themselves are now known to be remarkably stable even at the level of a few percent, and show no appreciable changes in response even after one year of flight.

However, IRAC exhibited a number of undesirable behaviors in-flight, many of which were either unanticipated, or under-appreciated in terms of severity. The majority of these effects are associated with bright objects (primarily stars). Due to the large size of the SWIRE fields it is inevitable that dozens of bright stars appear within the fields. Furthermore, SWIRE's relatively low redundancy (most common depth of coverage is four) and closely spaced epochs (typically a few days) significantly hinder simple dithering approaches to minimizing these problems. The latter spacing of the epochs is important because it prevents a sizeable degree of rotation between epochs, since the rate of rotation of the fields as seen by Spitzer is only roughly of order 1 degree per day. Since many effects are fixed in detector coordinates, rotation (and not translational dithering) would have been the ideal way to remove these effects.
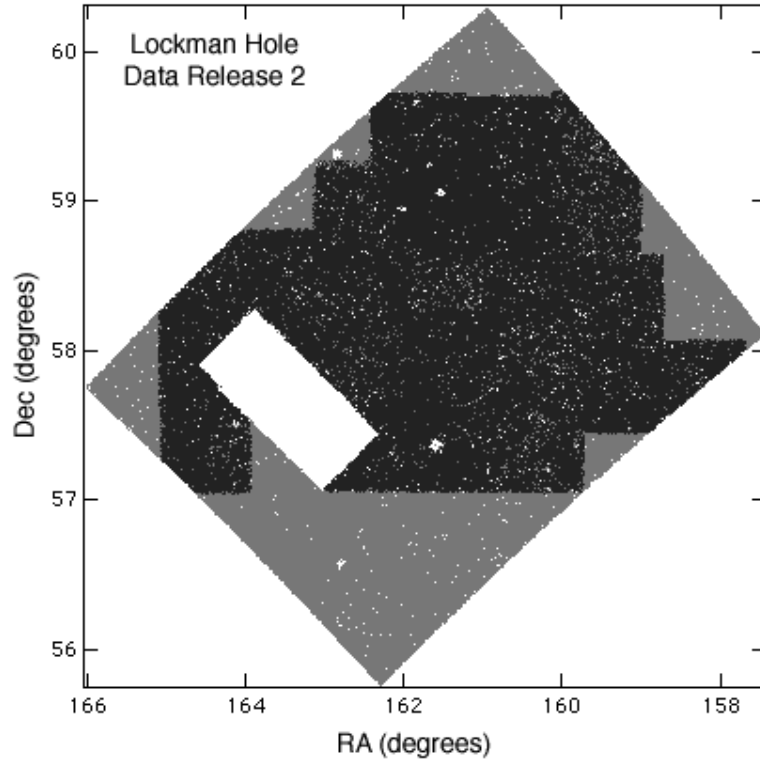
---

[7]http://ssc.spitzer.caltech.edu/mips/dh/

Fig. 20.— Location of the overlapping KPNO optical data relative to the Spitzer data. All Spitzer -IRAC detections are shown in grey, while those that were also identified with WFS optical counterparts are shown in black.

The data are therefore further processed on an individual frame-by-frame basis to *post facto* remove these effects. Specific effects treated are:

- *Column-Pulldown* - the column pulldown effect, which manifests in the slow read direction (columns) of the detectors at 3.6 and 4.5μm, is a depression in the zero-level of the column. It is detected based on statistical fluctuations in the columns, and then corrected by applying an additive constant to the affected column to match the background level in the rest of the frame. An additional mask bit is set per BCD which notes any pixels that have been corrected; these mask bits are preserved in the final mosaic mask image. There is a small amount of rotation between individual IRAC epochs, which combined with half-array offsets between epochs, is effective in at least minimizing this effect in many cases.

- *Muxbleed* - the muxbleed effect appears as a series of bright pixels along the fast read (horizontal in array coordinates) direction, and which may extend the entire width of the array (5$'$). In general, the SSC pipeline provides little or no correction for this effect. SWIRE processing provides an additional correction by fitting a linear function through the affected pixels, and subtracting the result while preserving the global background value. While this correction is poor for pixels immediately adjacent to the triggering pixel, for those located 10 pixels or more away the correction is effective. Like column-pulldown, a mask bit is set for corrected pixels.

- *Banding* - banding is encountered in the 5.8 and 8.0μm channels of IRAC. It is an electrical and optical effect in the IRAC detectors, and appears like a broad uniform band of light extending horizontally (in array coordinates) on both sides of a bright source. Like column-pulldown, banding is detected in the images based on statistical analysis of the rows in the image. It is corrected by fitting the rows and subtracting from them an additive constant. This constant is fit separately to the left, right, and within a specified radius of the triggering object. A mask bit is set for all corrected rows.

- *Short-Term Latent Images* - IRAC suffers from significant latent images. Fast timescale latents (which decay on timescales of minutes) are common and generally result from bright stars in the field. Objects likely to generate image latents are detected based on a thresholding scheme. Pixels so affected are tracked as a function of time, and masked during coaddition.

- *Long Term Latent Images* - the 3.6μm channel in IRAC suffers from image latents with extraordinarily long decay time constants. While the SWIRE fields themselves are generally free of objects which induce such latents, an examination of the data showed that up to 25% of the AORs had latents originating in other observations (from other Spitzer programs) that occurred prior to the SWIRE observations. Generally, our half-array offset dithering strategy in multiple epochs provides an effective means of partially suppressing the appearance of these latents. Because each IRAC AOR consists of hundreds of dithered observations, it was additionally possible to average all of the images together with outlier rejection to produce an image of the latents in that AOR. Such a latent calibration image was produced for every IRAC 3.6μm AOR, and was subtracted from the actual data prior to mosaicking and coaddition.

- *Background Matching* - IRAC has no ability to measure the absolute background, and this is especially true after the sky dark-subtraction implemented in the BCD pipeline. More vexing is that the actual brightness of the background changes as a function of time, as a result of the changing position of Spitzer and the relative location of the sun within the zodiacal cloud, which complicates coaddition of the data.

As a result, every BCD has it's median background level set equal to the predicted background for the field center on the midpoint of the data of observation of that field. This model is generated by SPOT, and is calculated from a COBE-derived model of the zodiacal cloud. As a result, the background seen in the SWIRE mosaics corresponds closely to what is expected for the actual sky background. **However, all structure on spatial scales similar to or larger than the array size have been removed.**

- *Position-Dependent Color Corrections* - Numerous corrections to the photometry of IRAC are required which depend on the exact position of a source on the array. The largest of these is a result of the varying angle of incidence of the incoming beam and the optical path through the detector filters. These result in an array-position dependent correct which is also color-dependent. The IRAC data is flat-fielded using images derived from the zodiacal background, which is very red. Although the perfectly flattens the background (which is dominated by zodiacal light in the SWIRE data), it is incorrect for bluer objects and can introduce flux errors of up to 10%.

  SWIRE data was corrected for this by first removing the diffuse background from the frames (see Background Matching above), and multiplying the BCDs by a correction image that accounts for the multiplicative factor between the zody flats and one appropriate for objects with a Rayleigh-Jeans slope. The background is then added back to the frames, and they are then mosaicked.

After individual processing, the data are mosaicked and coadded onto "tiles". The tiles vary in size from SWIRE field to SWIRE field, but are all the same for any given field and are roughly one square degree, with a subsampled pixel size of exactly 0.6″. The 0.6″ pixel size (which is very close to *but not exactly* one half the size of an IRAC native detector pixel) was chosen in order to resample onto a finer grid and thus to minimize aliasing with the large IRAC pixels, as the native IRAC pixels undersample the observed beam. The dithers used by SWIRE provide half pixel phase sampling. The one square degree tile size was chosen to provide an image size amenable to handling with current computing hardware; the full size field in unmanageably large. It was also chosen to provide a minimum number of tiles. The tiles are tilted with respect to the celestial coordinate system in order to align them with the overall rotation of the roughly square SWIRE field, thereby minimizing the amount of "blank" space in each tile (the overall rotation of the Spitzer field was dictated by the time of its observation). The individual tiles are deliberately designed with an overlap, such that objects falling onto a tile boundary cannot be lost. The BCDs pertaining to a given tile are gathered and then re-projected with the MOPEX mosaicking software developed by the SSC. All of the tiles share a common projection center, and are in effect subregions of a much larger virtual image. The data are coadded using an outlier rejection scheme that considers many different levels of outlier rejection. Bad pixel masks indicating permanently bad pixels are read. The additional masks generated by the SWIRE pipeline are read and used for pixel rejection of individual images. Outliers (generally cosmic rays) are rejected both on the basis of being inconsistent with the observed distribution of flux estimates for a given location on the sky (pixel outlier rejection), but also on a spatially filtered basis. Coverage maps, uncertainty images, and maskfiles are also produced.

Source Extraction

Sources were detected and extracted using the SExtractor software (Bertin & Arnouts 1996). Aperture fluxes were extracted within five separate apertures, which for IRAC range from 1-6× the full-width half maximum of the beam. A separate after-processor applies aperture corrections to the extracted fluxes and converts all units into physical units. The aperture corrections were derived from stars found in the mosaic
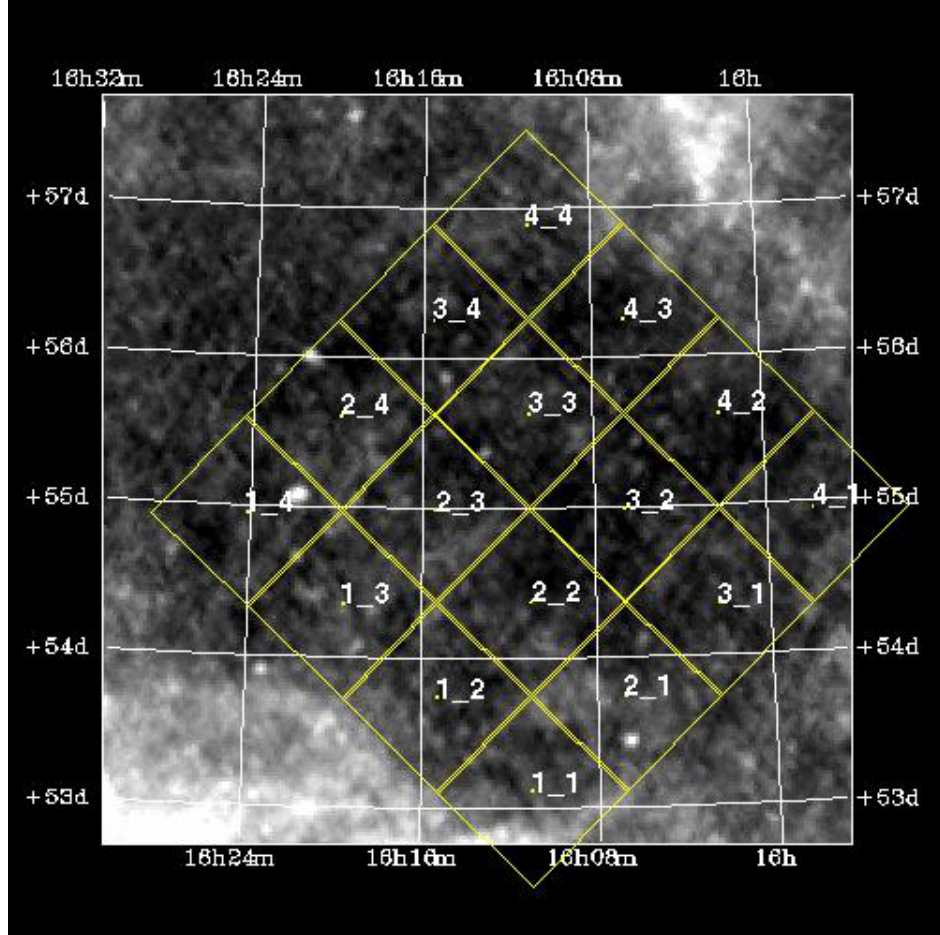
Fig. 21.— "Tile" system used for Spitzer -IRAC and optical data. The labels correspond to the filenaming convention, and also to the tile number as given in the catalog. The tiles are rotated with respect to the celestial coordinate system in order to align them with the orientation of the Spitzer data, thereby minimizing the number of tiles.

images themselves, to account for the difference in extraction apertures used for the photometry derived here and the calibration of IRAC. The aperture corrections were derived by constructing a composite point spread function from 10-20 stars in the field using DAOPHOT. Relative fluxes in different apertures were then measured from the composite PSF. The effective beam width (FWHM) measured from the composite PSFs were 1.9, 2.0, 1.9, and 2.2″. All fluxes given in the SWIRE Version 2 catalog are aperture corrected. The aperture corrections actually used are given in Table 9; these are consistent with those derived by the IRAC instrument team.

After extraction of the SWIRE catalogs, comparisons between photometry in different apertures for stars indicated that the aperture-corrected photometry within the three largest apertures agreed with each other to better than 0.5%. However, this was not the case for the smallest apertures. The differences are attributable to differences in how DAOPHOT and SExtractor measure fractional pixels. Therefore, the aperture corrections for the two smallest apertures were adjusted to force coincidence between them and the larger apertures, hence the high degree of quoted precision in Table 9.

Color-magnitude diagrams were constructed for various types of objects, in particular main-sequence stars. It was found that the scatter in these diagrams were minimized through the use of aperture 2, which is the 1.9″ radius aperture, and corresponds to roughly twice the beamwidth. *We therefore recommend the use of IRAC ap2.*

Filter	Radius(″)				
	1.4	1.9	2.9	4.1	5.8
3.6μm	0.585	0.736	0.87	0.92	0.96
4.5μm	0.569	0.716	0.87	0.905	0.95
5.8μm	0.465	0.606	0.80	0.90	0.94
8.0μm	0.419	0.543	0.70	0.875	0.94

Table 9: Aperture corrections applied to SExtractor aperture fluxes. Measured fluxes are divided by the above corrections.

In addition to the aperture fluxes, SExtractor provides numerous extended flux measures. Isophotal and Kron fluxes were also extracted, and are discussed further in Section 8.2.4.

6.2.2. MIPS 24μm Processing

All Basic Calibrated Data (BCD) image products were retrieved from the Spitzer Science Center Archive. One or two BCD-level reprocessing steps were performed depending on the field. The first, optional step, removed dark-latent temporal artifacts and was performed only for the XMM-LSS field. The overscans at 24μm for this field accidentally covered the bright infrared source Mira, leaving a trail of dark latent residuals in about half of the BCDs. The latents were corrected by a self-flattening technique in which time-ordered sequences of 100 images were medianed into correction flats, which were then normalized and divided into the corresponding BCDs. The second reprocessing step, performed for all fields, compensated for the varying background levels in the images, by computing the median of each BCD image (taking masking into account), and subtracting this constant from that image.

The reprocessed BCDs were mosaicked using the SSC's MOPEX software. As for IRAC, all images were reprojected onto a common tangent projection. Unlike IRAC, the MIPS-24 maps were made as one large

mosaic, instead of being broken into tiles, and the 24 μm maps have 1.2$''$ pixel spacing. Multiframe outlier rejection with 2.5σ thresholds was used to reject cosmic rays. The mosaicked maps include coverage maps but no uncertainty maps. (The large number of samples per point makes the standard deviation a more useful estimate of the uncertainty than propagating the SSC-provided uncertainties through MOPEX, and will be provided in future releases if the 24μm maps are remade.)

Source extraction was performed using SExtractor. Background estimation within SExtractor was done with a local background mesh size of 24 pixels and a background filter of 4x4 meshes. The detection threshold was set to 3.0$\times$ the rms determined by SExtractor, and a minimum of 5.0 pixels were required to lie above the threshold for a detection. The mosaic coverage map was used for inverse variance weighting. Aperture fluxes were measured in apertures with diameters in mosaic pixels of 8.75, 12.5, 17.5 and 25 mosaic pixels. Aperture corrections were derived by examining photometry of bright stars and comparing to the largest aperture. An additional factor of 1.15 was included for all apertures to match the procedure used by the MIPS instrument team to derive calibration factors from standard star observations. The values of the aperture corrections are 1.86, 1.61, 1.29, and 1.15 for these apertures. Finally, the values were divided by a factor of 0.96 to place the fluxes on a $\nu F_\nu =$ constant scale.

6.2.3. MIPS Ge SWIRE Processing

For both 70μm and 160μm, we coadded the default time-filtered BCDs ("fbcd.fits" files) from the SSC archive using the MOPEX software. The MOPEX software combined the data ignoring bad data flagged in the BCD mask files (bmask.fits) and the bad pixels define by the static pixel mask (pmask). Using the redundancy in the MIPS data, additional bad data values were removed via outlier rejection. The remaining good data were projected, correcting for array distortions, onto an output mosaic with pixels of 3.6$''$ at 70μm and 8$''$ at 160μm. Some earlier 160μm maps were released with 7.2$''$ pixels. For source extraction from the 160μm maps, we have determined that the maps with 8$''$ pixels aligned with the scan direction give the best results.

Source extraction was performed on the mosaics using the PRF-fitting capabilities of the MOPEX suite. For MIPS-Ge data, PRF fitting yields much more reliable results than aperture measurements for faint sources (e.g., as shown by comparisons of the FLS verification data with the FLS Main field data). The reduced chi-squared values give an indication of the goodness-of-fit. We made adjustments to the background-subtracted image and the uncertainty image, in the latter case to make the mean reduced chi-squared values close to unity. Extended sources and/or blended sources which are not well fitted with the PRF ($\chi^2 > 3$) have flux measurements that are typically underestimated. In addition, extended sources may be de-blended into 2 or more point sources. In cases of large sources, sources composed of multiple components, and/or sources with high chi-squared values, users may want to re-measure these sources with appropriate apertures to derive the total fluxes, i.e., **the MIPS-Ge catalogs are point source catalogs; no corrections have been made for extended or blended sources**. The completeness level of the MIPS-Ge catalogs has not been quantified, but these techniques have been shown to yield catalogs with high reliability based on the First Look Survey data.

The effective average point-source rms for the EN1 images is 3 mJy at 70μm and 25 mJy at 160μm. The noise is about 40-50% larger than expected at 160μm compared to the FLS data, which was reduced using the same techniques. The loss of sensitivity of the MIPS-160 SWIRE EN1 data may have resulted from the increased operating temperature of Spitzer at the time of observation around the safing event described

earlier.

6.2.4. Bandmerge of IRAC and MIPS-24μm Data

Bandmerging of the four IRAC catalogs and the MIPS-24 catalog was performed using the SSC's bandmerge software[8]. Briefly, this software computes for each band-to-band pairing a χ^2 value based on the position uncertainties for each source; then checks the linkages for consistency, falling back to second- or third-choice links if necessary. The final output of bandmerge includes only the "best" final linkages, such that a source from a given band appears only once in the merged list.

Our input catalogs included the centroiding uncertainties produced by SExtractor. These uncertainties are often unrealistic underestimates. Furthermore, these centroiding errors did not account for systematic uncertainties between arrays, and we found it necessary to also provide band-pair registration uncertainties to get acceptable merges. We specified 0.2-0.4 arcsecond uncertainties between IRAC channels, and 0.5-0.6 arcsecond uncertainties for all pairings of MIPS-24 with IRAC bands. The uncertainties were measured from the positional differences of the sources in an earlier iteration of the bandmerger.

The maximum value of χ^2 was set to 36 (the default). The combination of this value with the band-pair registration uncertainties allowed some unreliable merges–see Section 7.2.6 for details.

After bandmerge, the resulting catalog was loaded into a commercial database system. Subsets of the data can then be easily selected, such as the one that created the SWIRE release given here.

6.3. Optical Data

6.3.1. CASU Processing

The data were processed by the Cambridge Astronomical Survey Unit (CASU) as described in Irwin & Lewis (2001) and we provide here a short description of the reduction steps. The data are first debiassed (full 2D bias removal is necessary). Bad pixels and columns are then flagged and recorded in confidence maps, which are used during catalog generation. The CCDs are found to have significant non linearities so a correction using look-up-tables is then applied to all data. Flatfield images in each band are constructed by combining several sky flats obtained in bright sky conditions during the twilight. Exposures obtained in the i′ and Z bands show a significant level of fringing (±2% and ±6% of sky respectively). In order to remove this effect, master fringe frames are created by combining all the science exposures for each band. These fringe frames are then subtracted from the object exposures. After this removal, the fringing level is reduced to ±0.2% and ±0.4% of sky in the i′ and Z bands respectively. Finally an astrometric solution starts with a rough World Coordinate System (WCS) based on the known telescope and camera geometry and is then progressively refined using the Guide Star catalog for a first pass and the APM (Automated Plate Measuring) or PMM (Precision Measuring Machine) catalogs for a final pass. The WFC field distortion is modeled using a zenithal equidistant projection (ZPN; see Calabretta and Greisen 2002). The resulting internal astrometric precision is better than 100 mas over the whole WFC array (based on intercomparison of overlap regions). Global systematics are limited by the precision of the APM and PMM astrometric catalog

---

[8]http://ssc.spitzer.caltech.edu/postbcd/bandmerge.html

systems and are at the level of 300 mas. The object detection is performed in each band separately using a standard APM-style object detection and parameterization algorithm, described in Irwin (1999). Standard aperture fluxes are measured in a set of apertures of radius r/2, r, $\sqrt{2}$ r, 2r, and 2 $\sqrt{2}$r where r=3.5 pixels (1.2″) and an automatic aperture correction (based on the average curve-of-growth for stellar images) is applied to all detected objects.

Photometric calibration is done using series of Landoldt standard stars (Landoldt 1992) with photometry in the SDSS system. For each night a zero point in each filter is derived. For photometric nights the calibration over the whole mosaic has an accuracy of 1-2%. During non-photometric nights, in otherwise acceptable observing conditions, we find that the derived zeropoint systematic errors can be up to 10% or more. Although the pipeline usually successfully flags such nights as non-photometric it still leaves open the problem of what to do about tracking the varying extinction during these nights.

All calibration is by default corrected for the mean atmospheric extinction at La Palma during pipeline processing (0.46 in U, 0.19 in g′, 0.09 in r′ and 0.05 in i′ and z). Since adjacent camera pointings overlap by several square arcminutes sources in these overlapping regions can be used as magnitude comparison points. However, to use overlapping and hence in general, different CCDs, requires that any repeatable systematics due to, for example, slight differences in the color equations for each CCD, are first corrected for. Correcting for these is a three stage process. First the twilight flatfields are used to gain-correct each CCD onto a common system. However, since the twilight sky is significantly bluer than most astronomical objects, a secondary correction is made using the measured dark sky levels in each CCD for each filter to provide a correction more appropriate for the majority astronomical object. These corrections, unsurprisingly, are negligible for passbands on the flat part of the generic CCD response curves such as g′ and r′, and amount to 1-2% for the i′ and Z passbands. The measured dark sky values for the U-band were also consistent with zero correction though with less accuracy due to the low sky levels in the U-band images. Finally any residual offsets between the CCDs are checked for each survey filter using the mean offset between adjacent pointings on photometric survey nights. The only filters requiring significant adjustments to the individual CCD zero points at this stage are CCD3 for U (-3%) and CCD1 for Z (+3%).

Data from non-photometric nights can now be calibrated in one of two ways: the overlap regions between pointings can be used to directly tie in all the frames onto a common system, with extra weighting given to data taken from photometric nights; the stellar locus in various 2-color diagrams (in regions of low unchanging extinction like these) can be used to compare colors from all the passbands by cross-correlating the loci between any of the pointings. The color-color loci cross-correlations (actually made from a smoothed Hess-like version of the diagrams) give results accurate to better than ±5%. The final products include astrometrically calibrated multi-extension FITS (MEF) images as well as morphologically classified merged multicolor catalogs. These as well as extended information on the images and catalogs are publicly available from the WFS web page (http://www.ast.cam.ac.uk/w̃fcsur/index.php).

6.3.2.   Coaddition and Remosaicking

For convenience, the individual WFS images were then reprocessed at IPAC to coincide with the geometry of the Spitzer IRAC tiles. Zero-level (additive) corrections were made to each individual CCD in order to force the regions of CCD-to-CCD overlap to have a common bias offset. The images were then masked based on the confidence images generated by the CASU pipeline. After this step, each CCD image was reprojected onto the coordinate system of the Spitzer data. The reprojected images were then coadded

using the Montage software (Berriman et al. 2002)[9]. The resulting images have the same tile boundaries, rotation angle, and projection system and center as the Spitzer tiles. The pixel scale is one half the size of the IRAC tile pixel scale, owing to the smaller beam width of the optical data. If the data are binned 2×2, they will yield an image that is directly comparable to the Spitzer data.

Various artifacts remain in the data after this process. Individual cosmic ray events in some cases have survived the mosaicking process and are visible in the images. Not all CCD-to-CCD bias level offsets have been completely removed, and particularly in z-band this leaves an overall ripple in the background. Also visible, particularly at z-band, are fringes arising in the detector that have not been wholly flattened out. Finally, bright star artifacts remain. It should be noted that the derived optical magnitudes in the SWIRE catalog were not derived from these images, but rather from the original CASU data as described above.

6.4. Spitzer-Optical Cross-Identifications

The cross-correlation between the Ug′r′i′Z optical and the IRAC-24μm catalogs was undertaken using the Webcmp package of IPAC's Infrared Science Archive (IRSA). Webcmp is optimized for extremely fast cross-correlations by position between extremely large datasets. A search radius of 1.5″ was used for the cross-identifications (XIDs). Webcmp provides a goodness-of-match criterion for each potential match which is identical to the χ^2 parameter of bandmerge (see Section 5.2.4), and an enhanced match probability indicator, P, based on the match algorithm of NED, NASA/IPAC's Extragalactic Database[10]. Webcmp does not, however, automatically select the "best" match to each source in the input list.

For the SWIRE DR2 Catalogs we have retained only one optical match to each Spitzer source, that with the highest P value, because a robust analysis of the source confusion rate has not been undertaken at this time.

6.5. Catalog Construction

The primary drivers for preparation of the SWIRE DR2 Catalogs were twofold: (1) that the catalogs be highly reliable with a minimum of artifacts; and (2) that we provide to the community as extensive and complete a listing as possible consistent with the overriding consideration of source reliability. To this end extensive analysis and validation of the entire dataset was undertaken, to evaluate the lowest flux levels for which the automated data products could be held to the required levels of reliability.

The most important causes of source unreliability are: (1) artifacts associated with bright stars; and (2) source confusion coupled with the limited performance of aperture photometry methods (as opposed to PSF-fitting methods) in highly confused regions.

The majority of artifacts associated with bright stars were eliminated from the basic SWIRE catalogs by tuning SExtractor to avoid their close vicinity. The method is not fully controllable on a star-by-star basis, so the exclusion region can vary star-to-star and can be different for a given star band-to-band. This method therefore gives rise to two sources of catalog incompleteness which users should be aware of: (1) **bright**

---

[9] http://montage.ipac.caltech.edu

[10] http://nedwww.ipac.caltech.edu

stars are either missing from the SWIRE DR2 Catalogs, have distorted flux measurements, or are multiply detected; and (2) **a source near a bright star can have dropped fluxes in some bands due to uneven exclusion zones band-to-band**. Sources lying within a certain radius of a bright 2MASS star have been flagged in the SWIRE DR2 Optical-IRAC-24μm Catalog to aid users in identifying sources which may be affected by bright star artifacts or which may have lost a detection within an exclusion zone.

For artifacts outside bright star zones, the most robust way to automate a procedure which will eliminate the large majority of unreliable sources is to require a detection of a candidate Spitzer source in at least two bands. Therefore this is the primary requirement of a source to be included in the SWIRE DR2 Optical-IRAC-24μm Catalog. **For any source to be included, it had to be detected at both 3.6μm and 4.5μm. The thresholds for detection were an SNR of 10 at 3.6μm and 5 at 4.5μm, which translate to 10μJy in both bands for almost all of the survey area.**

For the detection at any band to be reliable it must lie above a given SNR. The translation from SNR to flux is not direct, however. For the SWIRE automated aperture photometry, it is a non-trivial matter to derive accurate measurements of the photometric noise, and subsequently SNR, at the location of each source, for two primary reasons: (1) noise can vary quite widely across the field due to coverage variations and to the varying temperature of the arrays for MIPS; and (2) source crowding can lead to contamination of background measurements by nearby sources. Therefore for the combined IRAC-MIPS24 catalog we have chosen to derive a coverage based "coverage-SNR", CSNR, for source selection purposes, by adopting a single value for the average noise level in each band, and multiplying by a factor proportional to the square root of the coverage (the number of times the location was scanned by the IRAC array) of each source. This measures the relative size of the flux of a given detection versus the expected size of a statistical fluctuation solely in the blank sky background. This number is not the same as dividing the measured flux by the flux uncertainty, which is an error estimate that also contains a Poisson component from the actual target flux. For IRAC, coverage varies across the field, and can be obtained by the user from the coverage maps included in the Image Atlas. For 24μm, coverage is essentially constant at 4 coverages, therefore the SNR threshold devolves, in this band only, to a uniform flux threshold. The lower flux limits are shown in Table 10. **Detections that fell below the flux limit for a given band were set equal to "null" in the catalog.**

Wavelength (μm)	Lower Limit (μJy)	Usage
3.6*	10	$\times\sqrt{4/C}$
4.5*	10	$\times\sqrt{4/C}$
5.8	43	$\times\sqrt{4/C}$
8.0	40	$\times\sqrt{4/C}$
24	450	Fixed
70	30 mJy	Fixed
160	200 mJy	Fixed

Table 10: Lower flux limits for inclusion in the SWIRE catalogs. Sources were *required* to be detected at 3.6 and 4.5μm. Fluxes at other wavelengths are given if they were detected above the given limit. C is the depth of coverage, which is equal to 4 for most of the survey, and may be as high as 16.

It is important to note that this CSNR threshold should not be interpreted to measure photometric accuracy. The best estimate of an individual source's photometric SNR is found by compar-

ing the cataloged flux, `flux_ap_lam`, and associated flux uncertainty, `uncf_ap_lam`, as derived by SExtractor.

For the MIPS 70 and 160μm catalogs, sources were included if their point source fluxes, derived using the PRF-fitting software package in MOPEX, exceeded the thresholds at 70μm and 160μm shown in Table 10. For 70μm we also required that the source flux was at least 5 times the estimated noise level to remove residual artifacts in regions of low redundancy. Sources on the edges of the mosaics were excluded. The results of automated source detection was validated by direct visual inspection, and the flux level thresholds (Table 10) were chosen to insure high reliability.

7. The Data Products

7.1. SWIRE Spitzer Image Atlas

7.1.1. IRAC

The Spitzer data are provided as a set of FITS files. Due to the sheer size of the fields, the data are organized as "tiles"; each tile consists of four wavelengths each, and 4 images per wavelength. The data products have filenames of the following form:

```
swire_FIELD_IC_tile_X_Y_v2_mosaic.fits
swire_FIELD_IC_tile_X_Y_v2_unc.fits
swire_FIELD_IC_tile_X_Y_v2_cov.fits
swire_FIELD_IC_tile_X_Y_v2_mask.fits
```

where FIELD is the name of the SWIRE field, X & Y are the location of the "tile" in the 4x4 grid shown in Figure 4, the I stands for IRAC, and C is the IRAC channel number. C has the values (1,2,3,4) corresponding to 3.6, 4.5, 5.8, and 8μm, respectively. The "v2" indicates that this is SWIRE release version 2. All of the images have been projected onto the same geometry, so there is a one-to-one correspondence between pixels in the four types of data product.

`mosaic.fits` - these are coadded, mosaicked images in units of surface brightness (MJy/sr). These are the data of most interest to most users. Users should note that the images are in units of surface brightness, not flux, although to first order the two may be converted by multiplication by the nearly constant pixel size. Please see the *IRAC Data Handbook* for a description of how to measure fluxes from this type of image. Pixels that have no flux estimate have the value `NaN` as provided under the FITS standard.

`unc.fits` - the uncertainty in each pixel, corresponding one-to-one to the flux image of the same name, in the same surface brightness units. The uncertainties are computed based on the data that went into that pixel, and include contributions from Poisson noise and read noise. This is *not* an image of the background noise. The uncertainty written to this image is not itself highly certain, but the overall relative weighting between pixels is expected to be reliable.

`cov.fits` - the coverage maps indicate the number of individual images that went into each pixel in the flux images. In essence, this is the number of individual sightings of that piece of sky. Note that because the images are reprojected there are small corrections made to this based on the relative weighting of the input frame pixels, hence the values in the image are very close to, but not exactly, integer values (for IRAC the most common depth of coverage is 4). At the SWIRE depth, confusion noise is not very significant and the noise in IRAC images decreases roughly as the square root of the number of input images. Hence the background noise is closely correlated with the coverage map.

`Mask Images` - images whose bits encode certain error states, or flag potential problems, in the accompanying flux images. Because the individual bits contain the data, **a simple masking algorithm based on a threshold level cannot be used to mask problem areas.** Table 11 presents the values of the mask bits which are likely to be of interest to users.

IRAC Tile Mask Bits		
Bit	Name	Description
0	radhit	MOPEX single frame radhit detection. The first three bits originate in the MOPEX software used for mosaicking and coaddition. Users should consult the MOPEX documentation from the SSC.
1	temporal outlier	MOPEX temporal outlier radhit detection.
2	dual outlier	MOPEX dual outlier detection.
3	pulldown	The affected column was corrected for the column-pulldown effect. A positive offset was added to the column.
4	latent image	The pixels had one or more samples rejected due to potential contamination from an image latent, arising from a bright star elsewhere in the SWIRE data.
5	muxbleed	One or more pixels at this location were affected by muxbleed, and were corrected by application of a model fit. Sources with affected pixels should be considered to have suspect fluxes and reliability.
6	banding	One or more samples at this location were affected by banding, and were corrected by application of a model fit. Sources with affected pixels should be considered to have suspect fluxes and reliability.

Table 11: IRAC Mask Bits.

7.1.2. MIPS

Unlike the IRAC data, the MIPS data are not tiled and are delivered as a set of images encompassing the whole field. At the wavelengths observed by MIPS, the beam is much larger, and hence the pixel size needed to sample the beam is much greater.The resulting mosaics are therefore of a much more manageable size. The data are supplied as:

```
swire_FIELD_MC_v2_mosaic.fits
swire_FIELD_MC_v2_cov.fits
swire_FIELD_MC_v2_unc.fits
```

where FIELD is the name of the SWIRE field and C is the MIPS channel number. C has the values (1,2,3) corresponding to 24, 70, and 160μm, respectively. The "v2" indicates that this is SWIRE release version 2. The mosaic, coverage, and uncertainty files are the same as for IRAC. No uncertainty files are provided for 24μm.

7.2. SWIRE Optical Images

The images are provided as a set of "tiles" corresponding to the tiles so designed for IRAC. Filenames have the form:

```
FIELD_opt_tile_X_Y_F_mos32.fits
```

where FIELD is the field name (EN1, EN2, or Lockman) ,X & Y refer refer to the tile number, and F is the

name of the observed filter. The "mos32" means "mosaic, 32-bits". The tile numbers correspond directly to the tile numbers used for the Spitzer IRAC data. The filter is one of $ugriz$.

The image headers contain the precise filter and filter system used. The header also in some cases contains the keyword MAGZPT. This is the mean magnitude zeropoint of the files that were coadded to make the tile. In general, users should use the provided catalog magnitudes rather than remeasuring their own, since these were measured from the original frames and have additional corrections applied.

7.3. The SWIRE Spitzer-Optical Source Catalogs

7.3.1. IRAC-24μm-Optical Source Catalog

As detailed in Section 5, the requirements for a source to be included in this V2 release are:

- The source must lie within the region of sky covered with high coverage levels in all four IRAC bands.

- The source must pass the CSNR-adjusted flux threshold with a value greater than $10 \times \sqrt{4/C}\mu$Jy at 3.6μm and $10 \times \sqrt{4/C}\mu$Jy at 4.5μm (see Section 5.5).

In addition to these inclusion requirements, a source can be excluded if it is a bright star or if it lies too close to a bright star, as detailed in Section 5.5.

Eventually, the catalogs will be available via the Infrared Science Archive interface. The IRAC-24μm-Optical Catalogs are ascii flat table files in standard IPAC Table format[11], and are entitled

SWIRE2_FIELD_cat_IRAC24_DDMMMYY.tbl.

"SWIRE2" indicates Data Release 2. DDMMYYY give the day, month, and year of the catalog generation. Each catalog has 156 columns, which are described here. They are ordered by increasing Right Ascension. IPAC Tables begin with comment lines, initiated with a backslash character. These describe the provenance of the Table.

Following the comment lines are a set of four header lines. Columns within the Table are delineated between pairs of | characters. The first header line gives column names and the second indicates the nature of the data in that column: character, integer, or double precision floating point. The third header line indicates the units for the column, where applicable. Finally the fourth header line indicates what value a null data entry in that column will be denoted by. For the IRAC-24μm-Optical Catalogs, nulls are always indicated by the numerical value of -99.

1. cntr (integer) is an internal record number from the master database table from which the sources were selected. It is included in the released Catalog for database linkage reasons. It is not useful as a sequential record number because it does not increase monotonically with Right Ascension, and because there are gaps in a sequential listing of cntr for the IRAC-24μm-Optical Catalog. However it is useful as a purely numerical source identifier within the Table.

---

[11]http://irsa/applications/DDGEN/Doc/ipac_tbl.html

2. `object` (character) is the name of the source, conforming to IAU standards. All sources in the IRAC-24μm-Optical Catalogs are labeled "SWIRE", followed by the integer "2" to denote that they belong to Version 1.0 of the SWIRE Data Products. The format for the numerical part of the name is the J2000 position of the object in hhmmss.ss+ddmmss.s format. Sufficient precision is provided in case subsequent versions of the SWIRE Catalogs achieve sub-arcsecond separation between close sources.

3. `ra` and `dec` (double precision floating point) are the Right Ascension and Declination of the source in J2000 decimal degrees. The position is the resulting output of the Bandmerge processor, as described in Section 6.2.4, and it is usually dominated by the higher precision and higher SNR 3.6 and 4.5μm source extractions. Positional uncertainties are not listed in this Table because they are dominated by systematic effects. This is described further in Section 8.2.5.

4. `tile` (integer) is a numerical label denoting the IRAC $\sim$1$\times$1 square degree tile which the source is found in. The tile labeling system is illustrated in Figures 4, 8, 12, and 16; the first digit of the label refers to row number and the second refers to column within the tile layout. Thus, for example, tile_1_1, the lower-left-most tile, is labeled as tile "11" in the Table.

5. `flux_apN_xx` and `uncf_apN_xx` (double precision floating point; μJy) are the fluxes and their uncertainties for the 5 Spitzer wavelength bands, where "xx" is 36, 45, 58, 80 or 24 to denote the 4 IRAC bands 3.6, 4.5, 5.8, 8.0μm and the MIPS 24μm band. "N" refers to the aperture number, where smaller numbers indicate smaller apertures; the actual aperture sizes are given in Section X. The fluxes are aperture-corrected aperture fluxes as described in Section 5.2.1. Null values for fluxes and their uncertainties are denoted by "-99.00". **A null flux value does not necessarily mean a source has a flux below the SWIRE sensitivity limit in this band**. There are three reasons a null value may exist: (1) non-detection to the limits of source extraction; or (2) failure of the detected source to meet the CSNR threshold criterion; or (3) lack of coverage in this band. The third criterion should not apply to null IRAC flux values since we have attempted to limit the IRAC-24μm-Optical Catalog to the full IRAC coverage area, but we do not guarantee this to be the case.

6. `flux_kr_xx` and `uncf_kr_xx` (double precision floating point; μJy) are the Kron fluxes and uncertainties computed by SExtractor.

7. `rad_kr_rad` (double precision floating point; $''$) effective Kron radius, computed from SExtractor's derived shape parameters and the Kron factor.

8. `flux_iso_xx` and `uncf_iso_xx` (double precision floating point; μJy) are the isophotal fluxes and uncertainties computed by SExtractor.

9. `area_iso_36` (double precision floating point; $''$) isophotal area used in derivation of the isophotal flux.

10. `stell_xx` (integer) are the single digit stellarity indices generated by the SExtractor software package, one per Spitzer band. They indicate how well the source resembles a point-like source. High values indicate a high probability the source is star-like. The reader is referred to the SExtractor documentation for further details. Users should note that the stellarity index is not reliable at low flux levels. As an example, Figure 22 shows that the stellarity index becomes ill-defined at 3.6μm near 200μJy. An analysis of stellarity and star vs. galaxy colors for the IRAC-24μm-Optical Catalog is given in Section 8.2.12.

11. `a_xx`, `b_xx`, and `theta_xx` (double precision floating point; $''$) semi-major and semi-minor radii and position angle. The following indicates the meaning of the flag, as taken from the SExtractor documentation:

SExtractor Flag Bits		
Bit	Name	Description
0	Bright Neighbors	the object has neighbors or adjacent bad pixels which may affect the photometry.
1	Blended Object	Object was originally blended.
2	Saturation	At least one pixel was saturated.
3	Truncation	Object was too close to an image boundary (this should not happen in SWIRE data).
4	Bad Apertures	Object's aperture data was incomplete or corrupted.
5	Bad Isophotes	Object's isophotal data are incomplete or corrupted.
6-7	Memory Overflow	Deblending or extraction caused a memory overflow.

Table 12: SExtractor Flag Bits (adapted from the SExtractor 2.3 User's Manual, E. Bertin)

12. `flgs_xx` (integer) - SExtractor generated status flags.

13. `ext_fl_xx` (integer) - source extension flag. A value of -1 indicates a definitely point-like object, a value of 2 indicates an object that is clearly extended, a value of 1 indicates an idea that *might* be extended, and a value of 0 is indeterminate. In general, objects with this flag set equal to one will have poor aperture photometry, and the Kron flux will be preferable. See Section 8.2.4 for further details.

14. `cov_avg_xx` (double precision floating point; images) average depth of coverage in units of independent images at the source location.

15. `cov_xx` (integer; boolean flag) flag indicating whether valid data at wavelength "xx" existed. The flag has a value of 1 if data existed, and 0 otherwise. This is useful for determining whether null flux values arise from a lack of data or a lack of detection.

16. `ra_opt` and `dec_opt` (double precision floating point) are the Right Ascension and Declination of the optical source which has been matched to this Spitzer source, in J2000 decimal degrees. These coordinates are a refinement done on the position of the detected source using the combined WCS of the images in the 5 bands.

17. `ap_m_x` and `msig_x` (double precision floating point) are the aperture-corrected aperture magnitudes and their errors, measured in a fixed aperture of 1.2″, for the five optical bands, where "x" is u, g, r, i, or z for the Ug′r′i′Z band set from the INT WFS data. Null values for fluxes and their uncertainties are denoted by "-99.00". **A null flux value does not necessarily mean a source has a flux below the plate limit in this band**. Instead there may be lack of coverage in this band. **There are optical coverage gaps within the full coverage IRAC field** not only due to the overall mismatch between the optical and IRAC coverage, **but due to gaps between the chips.**

18. `int_m_x` (double precision floating point) are the integrated magnitudes for the five optical bands, where "x" is u, g, r, i, or z for the Ug′r′i′Z band set from the INT WFS data. The total fluxes were calculated using a curve-of-growth technique, as described by Hall & Mackay (1984). Null values for integrated fluxes are denoted by "-99.00". **A null value does not necessarily mean a source has a flux below the plate limit in this band**. Instead there may be lack of coverage in this band. **There are optical coverage gaps within the full coverage IRAC field** not only due to the overall mismatch between the optical and IRAC coverage, **but due to gaps between the chips.**

19. fl_x (integer) are stellarity flags generated by the CASU pipeline, one per band, as described in Section 5.2. Unlike the SExtractor stellarities measured for the Spitzer sources, the fl_x flags are coded flags. A value of -1 indicates a star; 0 denotes a noise source; 1 indicates an extended object such as a galaxy; -2 indicates possible non-stellar but too faint to be sure; -3 indicates possible stellar but too faint to be sure; -8 indicates a possible cross-match problem between bands; -9 indicates saturation, Users should consult the WFS documentation for details.

20. xid_dist (double precision floating point) is the distance in arcsec of the optical match from the Spitzer source. The search radius was 1.5″.

21. 2mass_fl (integer) is a flag used to identify sources which lie close to a bright 2MASS star (flag value set to 1). If a source is found to lie within a given radius of a bright star then there is a possibility that in one or more bands its flux may be affected by artifacts from the star, or it may have missed detection altogether due to the exclusion zone of the SExtractor software. Caution should therefore be used in interpreting the spectral energy distribution of such a source. The radius used for setting the flag varies by star brightness; details are given in Table 13.
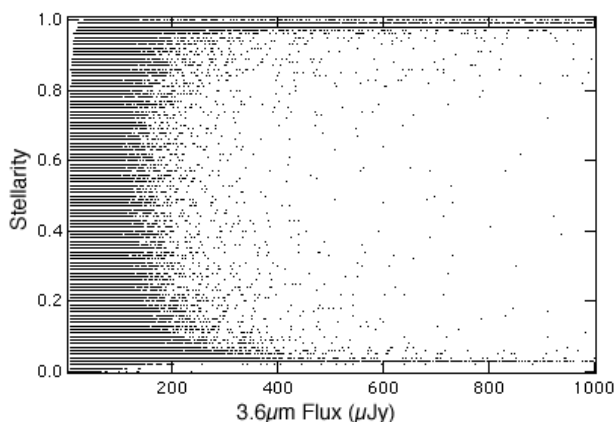
Fig. 22.— SExtractor stellarity index vs. 3.6μm flux. Below 200μJy the stellarity is poorly defined, and becomes a random number. Similar results are found for data at other wavelengths (with different limits).

7.3.2. MIPS Ge 70 and 160μm Source Catalogs

The MIPS catalogs at 70 and 160μm like the IRAC-MIPS24 catalog, are flat ascii text files in IPAC table format. Column details are provided in the headers of the catalogs.

As of this writing these catalogs are still being finalized. We anticipate the columns will include the following:

1. name (char) SWIRE source name.

2. RA (real) J2000.0 Right Ascension in decimal degrees.

3. Dec (real) J2000.0 Declination in decimal degrees.

4. `srcid` (real) internal source identification number.

5. `prf_flux` (real) Flux density in mJy from PRF-fitting.

6. `pflux_err` (real) Uncertainty in fitted flux.

7. `SNR` (real) Signal-to-noise ratio. Note that this is not simply flux divided by flux uncertainty

8. `Flag` (int) Flag indicating whether the source is near the edge (value of 3) or below flux limit (value of 2).

9. `redchi2` (real) Reduced chi-squared value. High values (greater than 2 or 3) for **bright sources** may indicate that an aperture flux should be used instead.

10. `apflux` (real) Several aperture fluxes will be provided (TBD). These should not be relied upon for faint sources.

7.4. Pseudo-Truecolor Images

New to this data release is a new data product, a set of pseudo-truecolor images for the IRAC data. A set of thumbnails (i.e. small images) create an easily viewed image of any given SWIRE field. These are supplied as standard HTML web-pages. Each thumbnail links to a full-size three-color image of a given tile. The three-color images were made by intensity scaling the data from each tile using a logarithmic transform, and mapping the 3.6, 4.5, and 8μm data onto the blue, green, and red channels, respectively. The three-color images are supplied in lossy JPEG format, and hence photometry cannot easily be extracted from them. However, because they present the spectral energy distributions of the objects in the field in a manner easily understood by the human eye, they are extremely useful for interpreting and locating features within the field.

The pixels in the jpegs correspond exactly to the pixels in the individual, tiled mosaic images. Therefore, the RA/DEC coordinates of objects in the jpegs may be determined using the WCS of the tiles. For convenience, header files are also supplied which contain the FITS header of the original 3.6μm mosaic tile. These may be read into the IDL "fitshead" routine and used for coordinate conversion. Additionally, the IRSA "Oasis" tool will directly read the jpeg/header file pairs, and treat them as astronomical data. Users are cautioned that when reading pixel locations from the JPEGs (for example, using the XV software) that the standard convention for jpeg images is for coordinate 0,0 to be at the top-left. However, in order to interpret the pixel locations properly, users must remember that the FITS convention places the first pixel at the bottom-left.

8. Product Validation and Characterization

8.1. The SWIRE Spitzer Image Atlases

Validation of the imaging was carried out in several ways. The data were processed independently via the wholly independent Montage and MOPEX software, and the results compared. This showed that the software independently arrived at the same image products. Furthermore, the images were inspected visually for defects resulting from incomplete outlier rejection, and the astrometric solutions were checked via catalog overlay.

8.2. The SWIRE Spitzer-Optical Catalogs

8.2.1. Photometry

IRAC

IRAC *Spitzer* data is calibrated by the SSC, and delivered in calibrated form to SWIRE. We have not performed any additional recalibration ourselves. We have, however, checked the calibration of the data products derived from the SSC BCD images in several ways.

A detailed photometric comparison was made to the 2MASS catalog. The bandmerged IRAC/MIPS-24 SWIRE catalog was cross-identified against the list of 2MASS sources in the ELAIS-N1 field. At fluxes greater than 0.5 mJy at 3.6μm many of the SWIRE objects are stars, which have a much smaller range in possible spectral energy distributions (SEDs) than galaxies, and in general stars appear nearly colorless in the Vega magnitude system. The K-IRAC colors were computed for each IRAC wavelength. It was found that the resulting colors for stars agreed with the model predictions to within 10%. Some of the disparity arises from the different colors of different spectral types of stars, which are readily apparent in the SWIRE data. Additionally, our different models disagree on the offset between the K-band and the IRAC filters. It was, however, found that the colors within the IRAC filters closely corresponded in both cases to the models. A similar result is derived from the photometric redshift determinations made by the SWIRE group for objects in the catalog. Fitting of SEDs for the template objects involved is expected (and in the past has) successfully shown underlying offsets in the photometric calibration, but the current catalog is predominantly free of these.

Second, a direct comparison was made to an independent deeper set of observations taken within the ELAIS-N1 region itself. This data was taken as a special part of the Extragalactic FLS program, and consists of two IRAC pointings, without overlap between the IRAC fields of view. Because the FLS-N1 data are much deeper than the SWIRE survey, faint sources in the SWIRE survey are detected at very high confidence in the FLS-N1. The deep FLS-N1 data therefore provides a "truth" set for comparison with the SWIRE data.

Each source in the SWIRE catalog was matched against it's counterpart in the independent deeper field. The resulting differences are shown in Figure 23. At the flux levels measured in this catalog, photometric differences between these two catalogs are generally around 9%, but it is believed that at least half this uncertainty arises in the extracted deeper catalog data. The systematic distortion in fluxes that existed in Data Release 1 has been eliminated - it was found to be tied to outlier rejection issues within the mosaicking software.

The new IRAC photometry differs from that in the ELAIS-N1 Data Release 1 by 0.0, 3.8, 2, and 6% at 3.6, 4.5, 5.8, and 8μm, respectively. All of the new photometry is *brighter* than the old photometry. Several factors have led to an overall recalibration of the IRAC data between these releases. These include a change to the definition of the IRAC calibration by the SSC, as well as bug fixes related to the handling of the IRAC pixel sizes.

MIPS

The calibration of the data were based on the current best knowledge of the instrumental performance, and validation of these data continue by the instrument team. The SSC 70μm S10 data were multiplied by 1.3 (recommended scaling factor for pre-bias change 70μm data, i.e., data observed before 2004 March). No
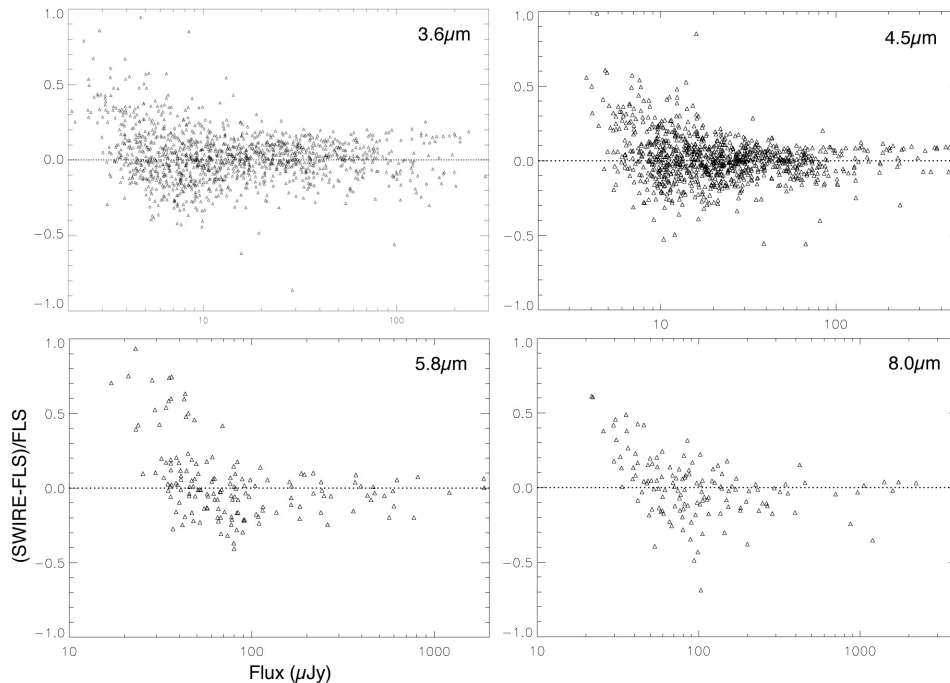
Fig. 23.— Detailed source-by-source comparison between SWIRE fluxes and those in the deeper FLS-N1 pointing.

calibration correction factor was applied to the SSC 160μm S10 data. No corrections were made for the electronic nonlinearity (1-2% effects) and no corrections were made for the flux nonlinearity (potentially 10+%) effects; the characterization of these nonlinearity effects are ongoing. Observers are encouraged to contact the SSC for the latest calibration and data issues. Given the current knowledge of calibration and the uncertainties with potential flux nonlinearities, we adopt an absolute flux uncertainty of 20% and 30% at 70μm and 160μm, respectively.

8.2.2. Saturation

Saturation is significant for stars seen by IRAC. Because IRAC is significantly undersampled, the exact flux limit as to when a source saturates IRAC varies considerably depending on the details of the beam center vs. the phasing of the array pixels. However, we can provide guidelines that will suffice for most users. The saturation levels (in flux units) for IRAC were determined by examining the 2MASS colors of objects identified as stars. At these wavelengths stars are all similarly colored. The point at which the 2MASS-IRAC color-magnitude diagrams deviate from stellar colors indicates the point of saturation. It is found that saturation begins to affect the IRAC channels at the greater than 1σ level at 23, 27, 39, and 34 mJy. This corresponds at 3.6μm to a K-band magnitude of 10.2. It should be noted that because the center (brightest) pixel of the IRAC PSF is a small fraction of the total flux, the effects of saturation are slow - stars considerably brighter (by 1-2 magnitudes) than these saturation points are only underestimated by factors of less than 20-40%.
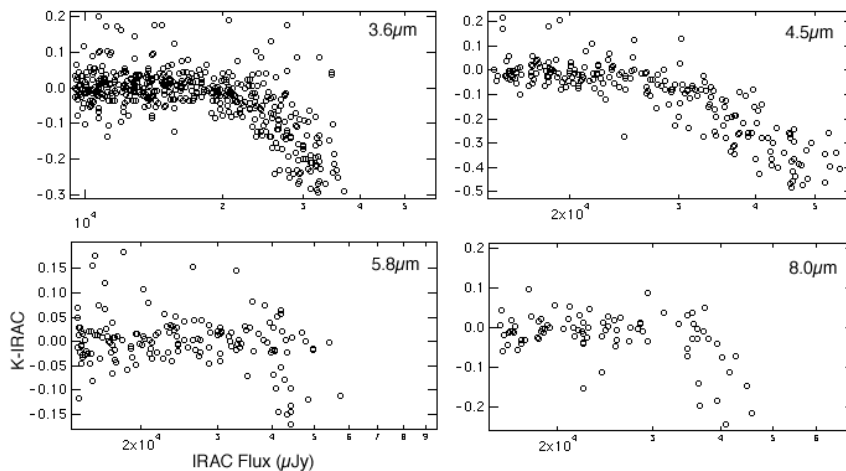
Fig. 24.— 2MASS K-band minus IRAC colors as a function of IRAC flux. The stars are nearly colorless at IRAC wavelengths; small offsets (<0.1) were applied to these colors to make them equal to zero in this figure.

8.2.3. Aperture Photometry

In Data Release 1, only aperture fluxes, in a single fixed aperture 2.9″ in radius was provided. However, for some uses this aperture was non-optimal. Furthermore, some users wanted to examine curves of growth for the sources in order to determine source extension and also to evaluate source confusion.

Therefore, Data Release 2 provides a set of five different apertures, both larger and smaller than those in DR1. These apertures are 1.4, 1.9, 2.9, 4.1, and 5.8″ in radius for IRAC, and 5.3, 7.5, 10.5, and 15″ in radius for MIPS-24.

8.2.4. Extended Source Fluxes

A significant change in Data Release 2 is the addition of flux measurements for extended sources. An examination of the Spitzer data, particularly for IRAC, reveals that large numbers of objects are obviously extended on spatial scales of 5-10″. Some are extended on scales of arcminutes. For these objects, the aperture photometry presented in Data Release 1 was clearly inadequate.

A "training set" was developed by examining tiles in ELAIS-N1 and identifying, by eye, galaxies that appeared either moderately or clearly extended. The isophotal area, stellarity, and flux were then examined in order to determine what region of parameter space these objects occupied. A set of limits were then chosen, and these were used to derive the source extension flag provided in the SWIRE catalog. It should be noted that the source extension flag is most certain for those objects set to "2", that is, these objects are certainly extended, and their fluxes are more accurately represented by the extended source fluxes rather than the aperture fluxes. However, note that there are likely many small, slightly extended objects for which the aperture fluxes are clearly underestimates, yet are too faint for us to measure accurately from the SWIRE data, or indeed to even tell if they are extended. Thus, many plots such as color-magnitude diagrams are likely to show a jump-discontinuity in them which is caused by the switch from point to extended source

fluxes. In addition to the source extension flag that we provide, users may examine SExtractor's several diagnostics to determine source extension: isophotal area, stellarity, and several measurements of source size. It should be noted that these various parameters have significant limitations. The most important caveats are that the stellarity value breaks down at low fluxes, and also that the isophotal area is strongly correlated with source flux.

The accuracy of the SExtractor fluxes was determined by measuring the fluxes of the training set objects by hand and comparing them to their SExtractor values. The results are shown in Figure 25.

Finally, it should be noted that the extended source fluxes are set on a *per-band basis*. For example, the Kron fluxes are determined at 3.6μm based on the Kron radius *at that wavelength*, whereas the Kron flux at 8μm is determined from the Kron radius at 8μm. As a result, the apertures are not matched and thus colors and spectral energy distributions derived from the extended source measures may not actually measure the same physical locations within a galaxy owing to the color structure inherent in many (particularly late-type) galaxies. The extended flux measures are the best choice when one seeks a "total" flux.

8.2.5. Astrometry

All SWIRE data products have been placed on the J2000 coordinate system.

The astrometry of Spitzer data is determined by two factors. First, all Spitzer data is tied to the pointing reconstruction derived at the SSC. This is done by merging the known pointing history of the telescope (derived from the onboard pointing control system, a combination of gyro and star tracker data) with the timing history of the instrument data collection. This level of pointing reconstruction is used for the SWIRE MIPS data. It is limited by knowledge of the spacecraft motion, scan mirror position, and other physical telemetry from the spacecraft.

IRAC data receives from the SSC pipeline an additional refinement based on forcing the observed image data to coincide with the astrometry of 2MASS. Sources are extracted on an AOR-by-AOR basis from the data, and correlated with the positions of 2MASS sources. Small adjustments are then made to the world coordinate systems of the IRAC BCD data. An analysis of the offsets between the star tracker and refined pointing showed a Gaussian distribution at 3.6 and 4.5μm, with a 1σ scatter of $0.2''$, and a small overall offset which results from known drifting behavior between the telescope boresight and the star tracker. However, at 5.8 and 8μm it was found that these same offsets formed a Lorentzian distribution centered around zero. Physically, however, these offsets should have mirrored those at shorter wavelengths. It would appear the current pointing refinement process fails the longer wavelengths, probably due to a paucity of available stars for the refinement, and the resulting offsets are simply noise.

These refined coordinates are used by SWIRE for IRAC 3.6 and 4.5μm data during reprojection and mosaicking, while at 5.8 and 8μm we used the star tracker (unrefined) pointing. It was found that the refined pointing in the longer wavelength channels often had erroneously large offsets, which resulted in bad positions in the resulting mosaics. The accuracy of IRAC astrometric reconstruction is generally free of systematics at the $0.1''$ level, with the registration of any given star accurate to roughly $0.3''$ (Barmby et al. 2004).

The accuracy of the registration can also be estimated by examining the distribution of positional offsets between cross-band identifications. Given that the separate extractions from different bands are presumably actually measuring the same object position, the offset is similar to the root squared sum of the underlying

positional errors. The positional accuracies derived from Figure 27 are consistent with positions for any given any source detection in any band being accurate to 0.2–0.4″, which is typically one-tenth to one-fifth of a beam.

An additional check was made of the MIPS Ge data by correlating the derived positions of the 70 and 160μm catalogs against the overlap between the Spitzer data and the SDSS. The median offsets were found to be 1″ at 70μm and 3″ at 160μm. The 90% confidence levels were at 4 and 8″, respectively.

8.2.6. Bright Source Artifacts

Bright source artifacts are a significant problem with Spitzer data. Most of these artifacts are discussed in more detail in the *IRAC Data Handbook*, available from the SSC. The following significant artifacts may be encountered in the SWIRE released data:

- Muxbleed - as detailed under data processing, muxbleed manifests as a series of small sources arranged linearly on either side of a bright source at 3.6 & 4.5 μm, with a spacing of 4.8″. The muxbled pixels may extend up to a maximum of 5 arcminutes on either side of a source, although for SWIRE they generally extend less than half this length. Their intensity varies with the flux of the triggering object, but they are typically many times the background noise value. This effect is corrected in Data Release 2. However, incomplete suppression may result in small lines of sources, similar to diffraction spikes (see Figure 28)

  Application of our multi-band detection criterion generally helps suppress muxbled pixels from the catalog. Observers are primarily warned that chance coincidence of a real source and a muxbled pixel, however, can lead to considerable overestimation of source flux in the affected band.

- Muxstriping - related to muxbleed, this effect results in a sizeable region near a bright star having a striped appearance, often with an overall offset in background level.

- Column-Pulldown - also described earlier, inaccurate removal of this artifact generally results in a cosmetic blemish in the immediate vicinity of bright stars. It looks like a small band of low background extending from a bright star, orthogonal to the direction of any muxbleed. This artifact has little if any effect on the source catalogs.

- Banding - this problem afflicts very bright sources at 5.8 and 8μm. It can extend up to 5 arcminutes on either side of a source. Data Release 2 corrects for this effect, and it has largely disappeared in this data release.

- Straylight -IRAC suffers from significant straylight issues, which mostly appear in the IRAC data when a bright star lands on a structure in the IRAC focal plane near the actual detector array. Because SWIRE has two epochs, displaced by half an array width, the stray light generally appears in only half the data. Unfortunately, the current outlier rejection scheme incompletely rejects the straylight, resulting in artifacting (see Figure 31). Third generation processing will include a prior model for the straylight, which will improve its rejection.

- Diffraction Rings and Similar Structure - the observed Spitzer PSF is very complex. At the shorter wavelengths, there are many scattering features similar to the diffraction spikes seen on ground-based telescopes. At the longer wavelengths, which have larger beams, the diffraction rings are not simple

anuli, but instead form what appear to be small discrete sources. In all IRAC bands, out-of-focus ghost images from filters may appear as a small ring a few arcseconds in diameter displaced by several tens of arcseconds from a bright source. Both of these features may result in erroneous detections of spurious sources (see Figure 30).

Our requirement that an object be detected in multiple bands is generally effective at removing such objects from the SWIRE catalog. Such features are generally found at different locations at different wavelengths.

Bright Object Flagging	
2MASS K mag. Range	Radius ($''$)
> 12.0	0
10.0 – 12.0	10
8.0 – 10.0	15
7.5 – 8.0	25
6.5 – 7.5	40
5.0 – 6.5	60
<5.0	120

Table 13: Lookup table used for defining the bright object flagging radius. Note that objects with this flag set are much less likely to be reliable than objects without the flag set.

As a convenience, a flag (`2mass_fl`) is provided in the catalog table to indicate proximity to a bright star. The flag has a value of 0 normally, and 1 if the given source lies within a fixed radius (see Table 13) of a source from the 2MASS catalog, as a function of K-band magnitude. 2MASS was used for this purpose because very bright stars do not have reliably extracted fluxes in the SWIRE catalog, and may occasionally be split into multiple fainter sources, or are saturated and so no flux can be well-measured. Since any object triggering bright star artifacts in the SWIRE data is easily detected by 2MASS, which has reliable fluxes even for very bright objects, it was better to use for this purpose. Note that this flag masks a circular region around each bright star. This radius was set primarily to inhibit artifacts resulting from erroneous detection in the wings of the PSF. Some artifacts which can extend for fully 5 arcminutes, like muxbleed and banding, may fall outside this region.

8.2.7.   Completeness

The completeness of the Data Release 2 SWIRE catalog IRAC data was evaluated by comparison to deeper data. First was a direct comparison to a deeper field taken within the ELAIS N1 region. These data were taken as a special part of the Extragalactic FLS program, and consist of two IRAC pointings, without overlap between the IRAC fields of view. Because the FLS-N1 data are much deeper than the SWIRE survey, faint sources in the SWIRE survey are detected at very high confidence in the FLS-N1. The deep FLS-N1 data therefore provides a "truth" set for comparison with the SWIRE data.

The SWIRE and FLS-N1 data were compared source-by-source over an area of 25 square arcminutes. We present in Figure 32 the integral completeness curves derived from this comparison. At each point is shown the percentage of objects with fluxes *actually reported* in a given band, vs. the total number of sources

detected at that band in the deeper data. At these flux levels, incompleteness in the deeper data is negligible. Note that in general objects at the longer wavelengths actually appear in the SWIRE images, but that due to the flux cuts applied to the delivered catalog the fluxes are listed as null. The 95% completeness level occurs at 14, 15, 42, and 56μJy in IRAC bands 1–4. These values are likely dominated by the very rapid falloff in completeness near our flux thresholds.

Additionally, we have examined the differential source counts as a second means of verifying the completeness of the SWIRE IRAC data. A detailed analysis of source counts in the SWIRE fields is forthcoming in Surace et al. (2005). In Figure 33 are reproduced some relevant portions of those results. Shown are differential source counts in each of the IRAC bands. Also shown are the counts from the SWIRE master catalog, from which the release catalog was drawn and which is somewhat deeper than the release catalog. Also shown are the counts from Fazio et al. (2004), which arise from a multi-depth survey with IRAC and extend to much greater depth than shown here, and counts from an extremely deep observation near the north ecliptic pole, to be detailed in Surace et al. (2005). The location of the turnover and break from the power-law nature of the deeper counts by the SWIRE release catalog (closed circles) indicates the loss of completeness in the catalog. These are observed to occur near near the expected flux thresholds.

At 24μm the overlap of SWIRE sources with the FLS field in EN1 is too small for meaningful statistical comparison. 24μm completeness has been estimated using simulations to add sources to the existing mosaic, and SExtractor to extract all sources. Completeness estimated from this procedure is greater than 97%. Details will be published in a forthcoming paper (Shupe et al. 2005 in preparation).

Finally, we show in Figure 34 the histogram of fluxes found in the combined IRAC-MIPS24 catalog. As expected, the fluxes peak near the adopted flux threshold. Some variation is noted due to the actual distribution of SEDs of the sources. There is a tail below the cutoffs in the IRAC bands, due to sources that lie in high coverage regions and which therefore have higher CSNR than if they had been in another part of the survey.

8.2.8. Reliability

Reliability is defined as the percentage of sources which are actually real, as opposed to spurious sources such as artifacts. This is different from accuracy, which measures how well the fluxes were measured. Reliability of the catalog has been enforced by requiring multi-band detection for all catalog entries, specifically at 3.6 and 4.5μm. The primary sources of unreliability in the SWIRE image data are bright star artifacts. However, these artifacts rarely occur in the same location (if at all) between different bands.

Reliability was determined through two means. The first was by direct inspection of subsets of the catalog. The subsets were regions in the SWIRE field chosen to lie at the centers of the the tiles. Since these were arbitrary locations, the results should not be biased (by avoiding bright objects, etc) to be significantly different from the catalog as a whole. All sources in the SWIRE catalog were examined at every available wavelength. Results of this examination indicate a reliability >99%. the MIPS 24μm data was further manually inspected, and spurious and questionable sources were nulled in the bandmerged catalog by hand. The reliability of the 24μm detections is also above 99%.

The second method was via examination of the observed spectral energy distributions of the SWIRE objects. Objects found in the deeper master catalog were deemed reliable or not based on the correspondence between their observed SEDs and those of known objects. The catalog as drawn using our CSNR criteria

was found to be highly reliable when cross-correlated against the list of reliable objects based on their SEDs.

Users are strongly urged to consider that **while the SWIRE catalog as a whole has a reliability greater than 99%, many conceivable sub-selections of targets from the survey will be much less reliable**. In particular, selections made on the basis of peculiar or unusual colors are much more likely to select for objects with suspect reliability. For this reason, users are strongly urged to consider their selection criteria, and to always be sure to examine the provided images. In other words, one should remember that catalogs are a derived data product, not the actual data themselves.

8.2.9. Bandmerge Completeness and Reliability

Bandmerge completeness is difficult to define, let alone estimate, and is not treated in detail in this document. Bandmerge reliability may be estimated by examining the positional offsets between bands in each merge. A plot of the cumulative distributions is shown in Figure 34. Figures 35 & 36 show the distribution of radial offsets between cross-band merges.

In greater than 90% of the cases, the sources in the merge are within 1.5 arcseconds for IRAC channel-pairs and within 3 arcseconds for MIPS-24 to IRAC pairs, and can be considered reliable. Of order 0.5% of IRAC Ch1-Ch2 merges and MIPS-24 to IRAC merges are too far away to be reliable.

8.2.10. Spitzer-Optical Cross-Identification Completeness and Reliability

We have investigated the completeness and reliability of the cross-identifications (XIDs) between Spitzer and optical sources in the SWIRE V1 ELAIS-N1 IRAC-24μm Catalog by performing a random match experiment to determine the rate of false matches. The maximization of completeness and reliability (C & R) for XIDs is usually a trade-off because increasing the completeness means increasing the accepted match search radius past the distance where an appreciable level of unreliable matches intrudes into the sample. We have chosen to maximize completeness at the expense of reliability, therefore the user should **beware of false XIDs in the Catalog, especially at faint optical magnitudes**.

To study the C & R distributions of the XIDs, the complete list of all Spitzer sources in tile_2_2 was shifted in position by 5 arcminutes and then re-matched to the optical catalog. For this experiment a search radius of 3 arcseconds was used for both the true position and false position cross-identifications, so that the tail of false matches to large distances could be determined.

The analysis is based on the Likelihood Ratio goodness-of-match parameter, which measures the probability that the true optical match lies distance d from the Spitzer source to the probability that a false match lies at distance d. LR is defined as:

$$LR = (e^{-r^2/2})/4\pi N(<m)\sigma$$

where r is the separation of the two sources measured as a fraction of the combined positional uncertainties of the optical and Spitzer source, σ, and $N(<m)$ is the integrated number density of optical sources on the sky brighter than the magnitude, m, of the match candidate in question (see Rutledge *et al.* (2000) for a detailed discussion of the LR method adopted here.)

The resulting distributions of LR for the false and true matches are shown in Figure 37. Here we plot the LR value for every optical source that fell within a circle of radius $3''$ around each Spitzer source in tile_2_2. The true position run is indicated in black and the false position run in red. It can be seen that LR values below about 0.5 reflect purely random, false, matches, while an LR value of 3 or higher is required to be confident of a high reliability match.

The LR value for a Spitzer-optical match varies not only with distance between candidate matches but also on the magnitude of the candidate match; since source counts increase with increasing magnitude, it is more likely that we will find a faint confusing background source in the search radius than a bright one. Another reason LR depends on flux density, in both the optical and the Spitzer bands, is that lower SNR sources may generally have less well measured positions so they cannot attain LR values as high as those for brighter sources with more accurately measured positions.

In Figure 38 we illustrate the effect of match magnitude on LR. We plot LR vs separation (xid_dist in the Catalog) of each candidate optical match to each Spitzer source, color coding the points by r′ magnitude of the optical match, for both the true and the false Spitzer position samples. Here we see that at a given separation, fainter match candidates attain systematically lower LR values than brighter ones, as expected. We also see that above the lower reliability limit LR∼0.5, below which matches have essentially zero reliability (Figure 38), a bright match might have a separation as large as $1.8''$, but an r′ > 23 mag. source must be closer than about $1.1''$ to exceed this LR threshold.

These figures may be used to estimate the match reliability of an optical source with a given magnitude and given separation, xid_dist, from the Spitzer source.

For the cross-identification window that has been selected for the SWIRE V1 ELAIS-N1 IRAC-24μm Catalog, $1.5''$, it is apparent that the Spitzer-optical cross-identifications are essentially 100% complete, except possibly a few bright true matches at large separations might be missed. We point out the caveat that there are gaps in optical coverage so not all potential optical counterparts exist in the optical catalog.

The reliability of the cross-identifications is not 100% within the selected $1.5''$ search radius, since we see in Figure 38 that some matches with 1.1<xid_dist<1.5 can fall below the LR threshold of ∼0.5, below which match reliability is zero. Moreover reliability does not reach high levels until LR>3, where many optical match candidates are separated less than $1''$ from the Spitzer source.

The analysis presented here is a preliminary one and a global one. It does not take fully into account varying positional uncertainties with flux, nor clustering of sources. Therefore it should be used as a guide only to the reliability of matches as a function of separation and magnitude. The V2.0 SWIRE Data Products will incorporate an improved analysis and correction of systematic positional offsets between the Spitzer and optical catalogs, and will review the dependence of XID reliability on other factors. We will also address issues of local source confusion more deeply, and investigate methods to preferentially reject false matches.

8.2.11. IRAC Position-Dependent Gain Correction

IRAC is known to have a strong color term that varies across the field of view. The data is flat-fielded using observations of the zodiacal background which are much redder in the mid-infrared than the majority of sources observed by SWIRE, and in particular have a very different spectral slope than the stars used to calibrate IRAC. As a result, objects with SEDs similar to that of stars show a significant variation in flux depending on their location on the array. In short, the flat-field is incorrect for targets that differ significantly

in color from the zodiacal background.

SWIRE corrects for this effect by applying a position-dependent gain-correction appropriate for point-like objects with a stellar-like SED. The majority of objects detected by SWIRE fall into this category. In principle, while this should correct all the photometry for stars and early-type galaxies, it will result in errors of a few % for very red late-type galaxies.

The SWIRE data-taking strategy, which uses half-array offsets, is nearly optimal for minimizing this effect. Shown in Figure 39 is the effective correction, as derived by mosaicking the corrections based on the actual data pointings. For almost the entire field the correction is less than 1%. However, in a few small regions a confluence of the dithering and the correction map may lead to corrections as large as 10%.

λ (μm)	1σ correction (%)	mean (%)	min (%)	max (%)
3.6	0.5	0.0	-3.3	1.3
4.5	0.6	0.0	-4.3	1.5
5.8	1.4	-0.9	-8.8	2.6
8.0	0.9	-0.3	-6.0	2.6

Table 14: Position dependent gain corrections for the SWIRE IRAC dither pattern.

8.2.12. Star-Galaxy Separation

Stars dominate the SWIRE survey at bright flux levels. Above a 3.6μm flux of 1 mJy, stars constitute 50-80% of the total number of objects at 3.6 and 8μm, respectively. A detailed method for predicting which objects are stars will be presented in Surace et al. (2005), which determines number counts in the SWIRE fields. Future versions of the SWIRE data products will contain a star/galaxy discriminator. However, to first order users may make use of two characteristics of stars: they are pointlike, and they occupy a very narrow locus of colors compared to galaxies, particularly in the infrared.

Stellarity indices and flags are provided with both the infrared and optical data, respectively, to indicate whether the extracted source is extended or not. Users should note that these are not reliable at faint flux levels, and provide no real information. However, for brighter sources, they can be used to determine which objects are *not* stars. Also, the stellarity flags at optical wavelengths are more useful than the Spitzer stellarity indices, since their spatial resolution is at least a factor of two higher.

Colors (i.e. spectral shapes) also provide a powerful discriminator between stars and other objects. At IRAC wavelengths, stars are nearly colorless (relative to Vega) as these wavelengths are well on the Rayleigh-Jeans side of the spectrum. The locus of stellar colors is readily apparent in the $f_{3.6\mu m}/f_{4.5\mu m}$ vs. $f_{3.6\mu m}$ color-magnitude diagram (Figure 40). The mean is 1.68 with a 1σ scatter above 1 mJy of 0.11. A useful color requirement is that a given source must have a flux ratio in order to be a star that is within 3σ of that measured from the data, i.e. $1.35 < f_{3.6\mu m}/f_{4.5\mu m} < 2.01$. While this color cut might exclude some dwarf stars with peculiar colors due to molecular absorptions, it is useful for ensuring that bright, unresolved extragalactic objects will not be discarded as stars. Note that this requirement is necessary for an object to be a star, **it does not exclude galaxies** since the locus of galaxy colors includes the color space occupied by stars.

An additional color cut involves the optical r$'$ and i$'$ band fluxes, when available. Segregating the main

sequence in the [r$'$-i$'$]–[i$'$-3.6] color-space produces a distribution of stars well matched to expected theoretical models for stellar number counts. See Rowan-Robinson *et al.* (2004) for further information.

Users are cautioned to be aware of two things at this time. The number counts of stars below 100μJy remain poorly understood at this time, and the efficacy of our color/stellarity discriminators described above remain unproven. Second, the very brightest stars often have unreliable photometry and stellarity indices, so very bright objects must be examined by hand.
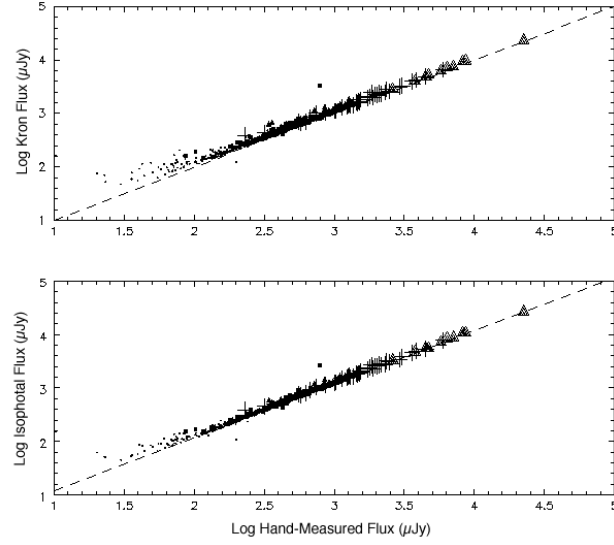
Fig. 25.— Comparison between extended source fluxes (isophotal and Kron) and the fluxes measured by hand at 3.6μm.
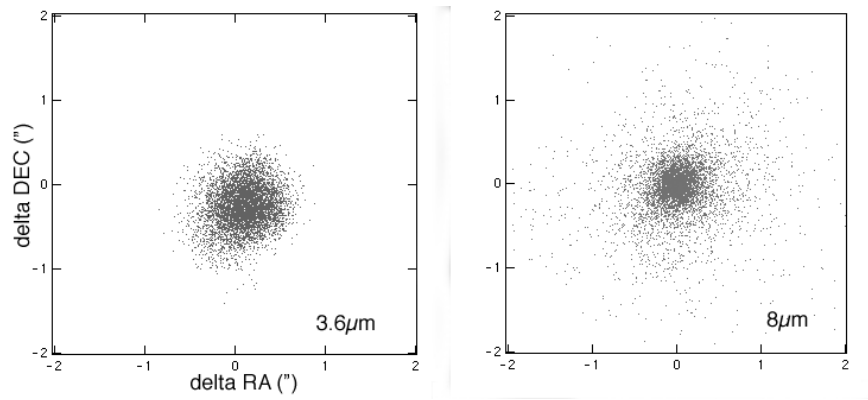
Fig. 26.— Offsets between the refined and star tracker pointing for individual BCDs from the same AOR at 3.6 and 8μm.
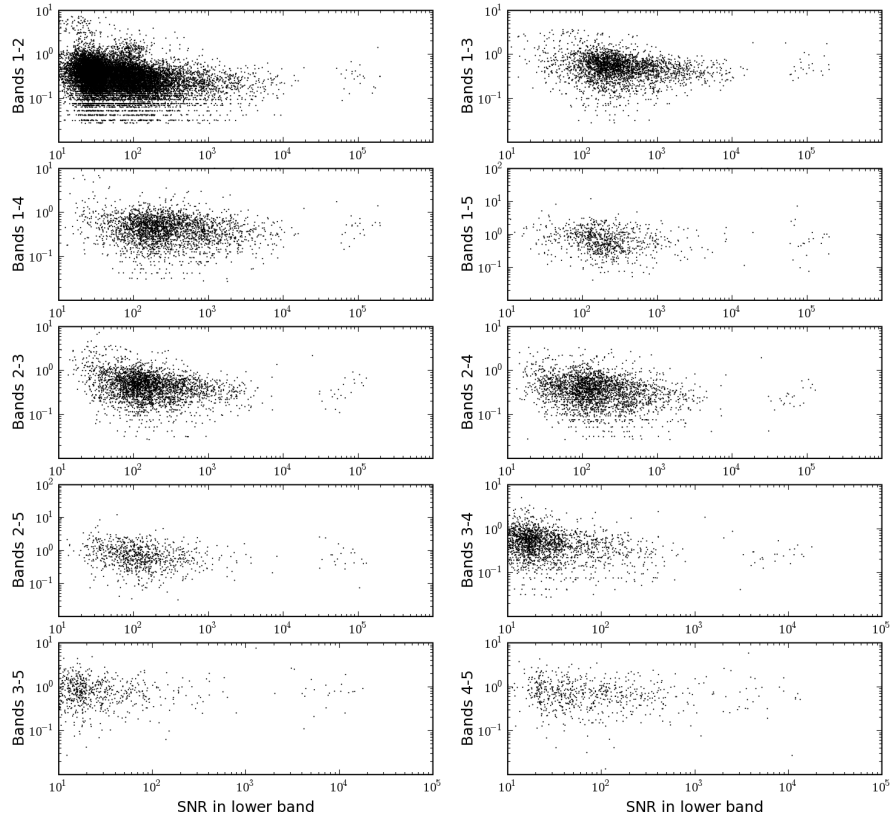
Fig. 27.— Scatter (arcsec) in cross-band positional offsets between cross-identified objects in the SWIRE catalog. Bands 1–5 refer to 3.6, 4.5, 5.8, 8, and 24μm, respectively.
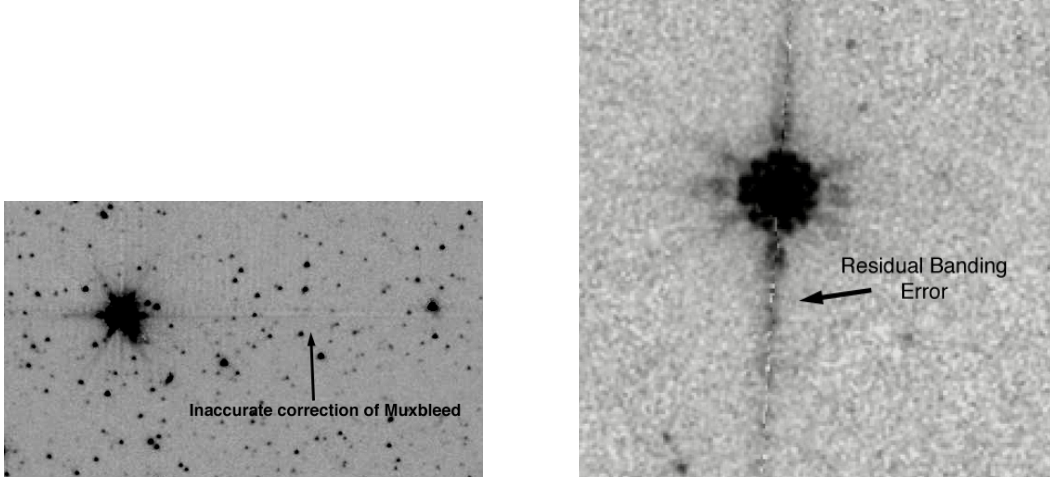
Fig. 28.— (Left) Examples of residual artifacts from column-pulldown and muxbleed, in ELAIS N1 tile_2_3, 3.6μm. (Right) Incomplete removal of the banding artifact, from tile_2_3, 8μm.
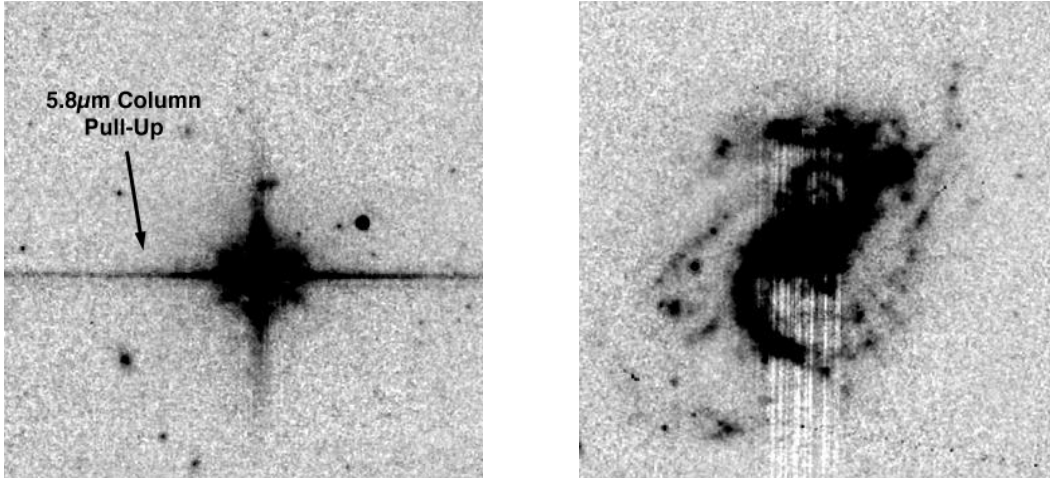
Fig. 29.— (Left) The IRAC 5.8μm channel displays a column-wise elevation in DC level. No correction has been applied in Data Release 2. (Right) Erroneous banding correction at 8μm resulting from very large object extension. SWIRE processing is optimized for point sources, and in a few instances the bright artifact correction is applied incorrectly.
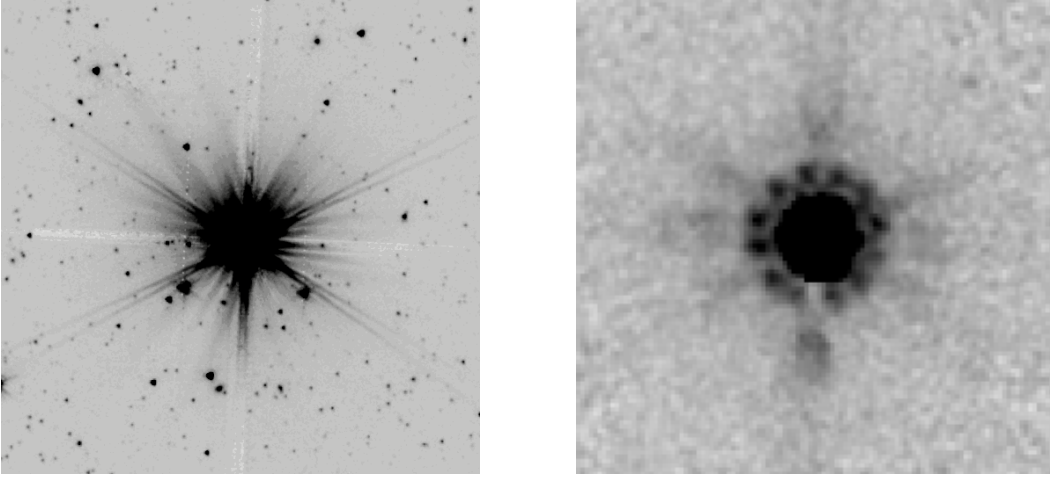
Fig. 30.— (Left) complex scattering structure in the 3.6μm PSF. (Right) Airy ring at 8μm. Both structures may trigger erroneous source extraction.
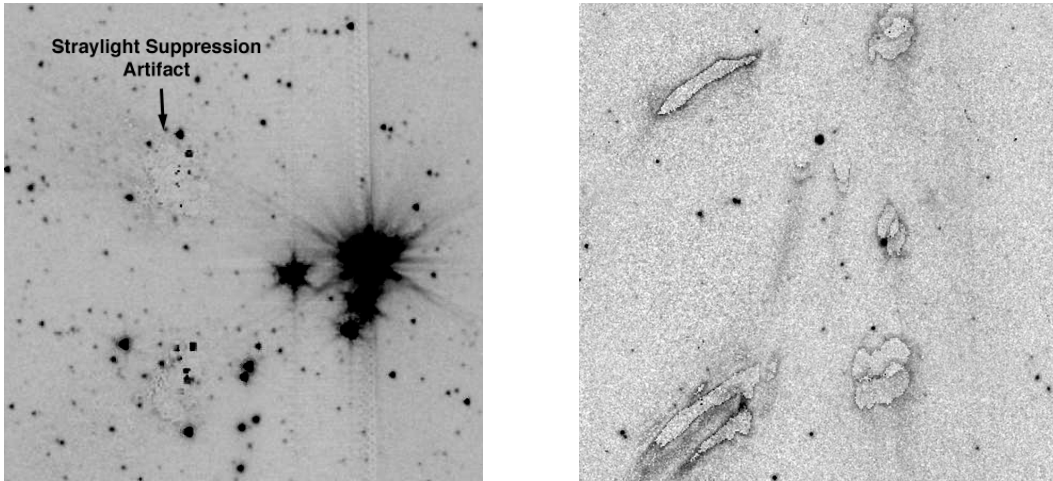
Fig. 31.— Incomplete rejection of straylight in IRAC. At left is one such example at 3.6μm. At right is the worst such example in the dataset, caused by straylight from the star Mira in tile 2_4 at 8μm.
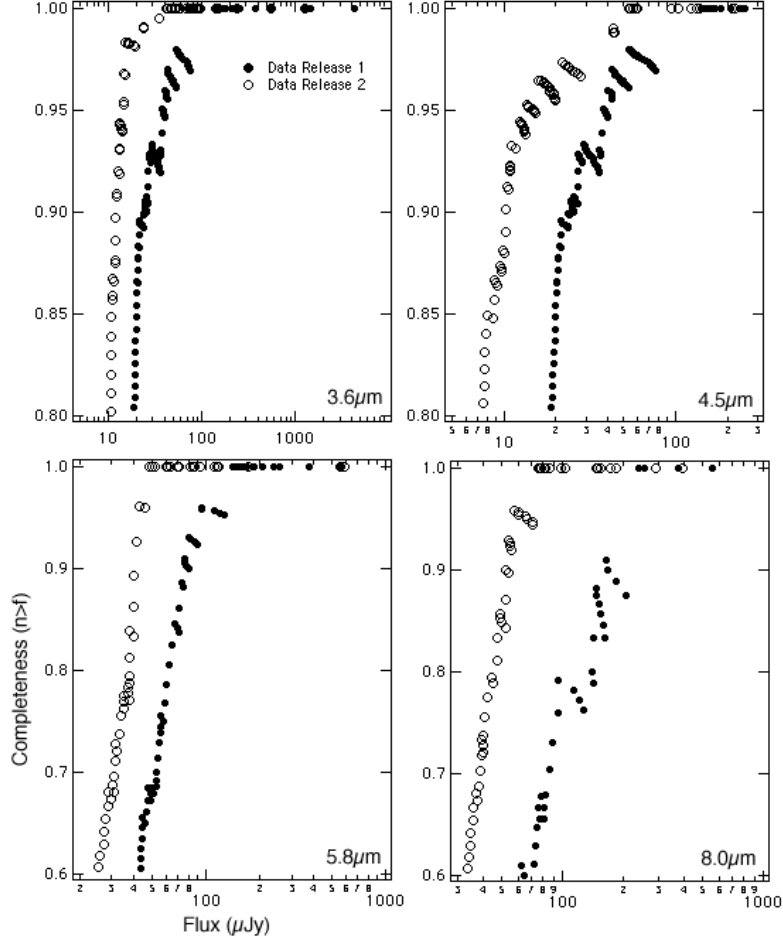
Fig. 32.— Integral completeness of the Data Release 2 SWIRE ELAIS N1 catalog for IRAC. The curves are derived from a source-by-source comparison with a deeper set of images taken within the EN1 field. The zig-zag nature of the curves is due to small number statistics above a given flux inside the limited area of the deeper field. The second data release is much deeper than the first, in large part because the flux cutoff in channel 1 was lowered by a factor of two.
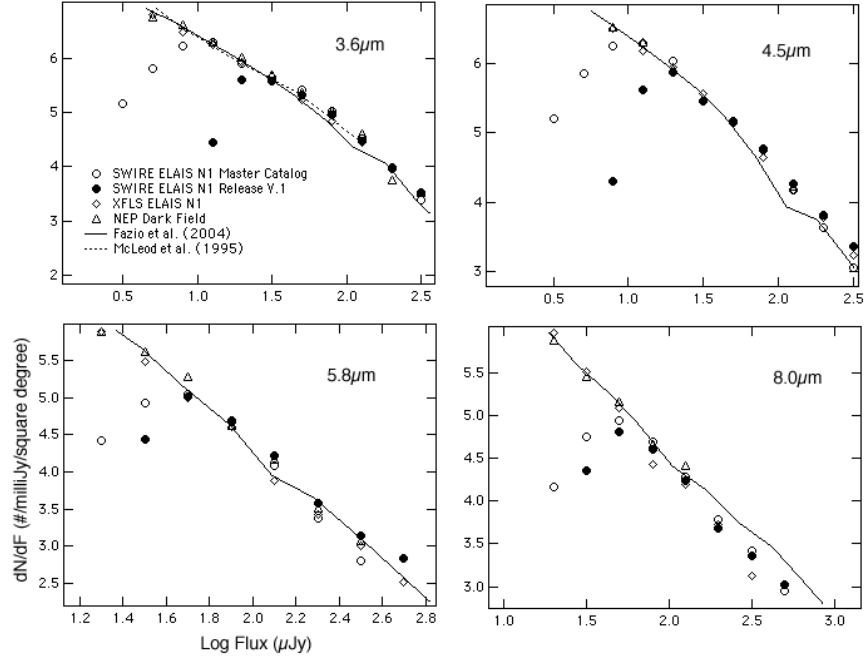
Fig. 33.— Differential source counts for the released SWIRE catalog compared to other counts taken from Surace et al. (2005). These include the deeper counts of Fazio et al. (2004), McLeod et al. (1995), and deeper surveys in the north ecliptic pole and as part of the extragalactic FLS in ELAIS N1. The break from the observed power-law distribution observed in the deeper surveys by the SWIRE release catalog (closed circles) illustrates the catalog's effective completeness limit.
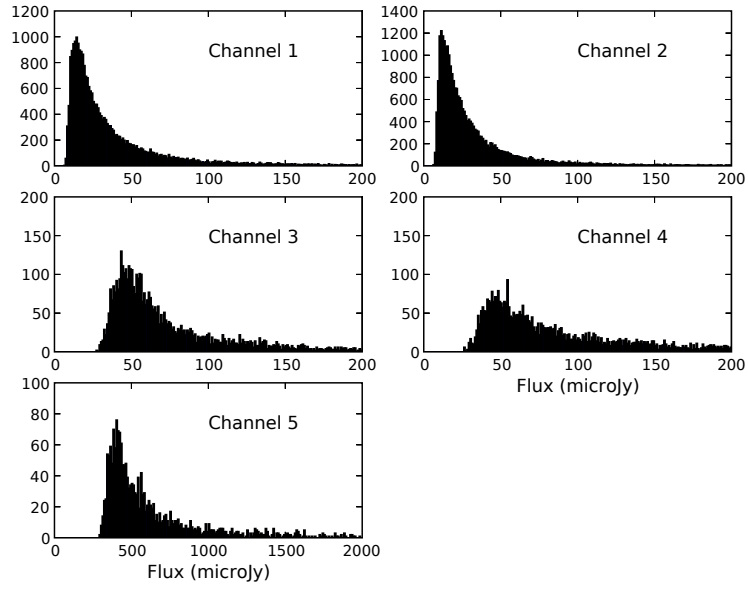
Fig. 34.— Histograms of fluxes in tile 22 of the combined EN1 IRAC-MIPS24 catalog.
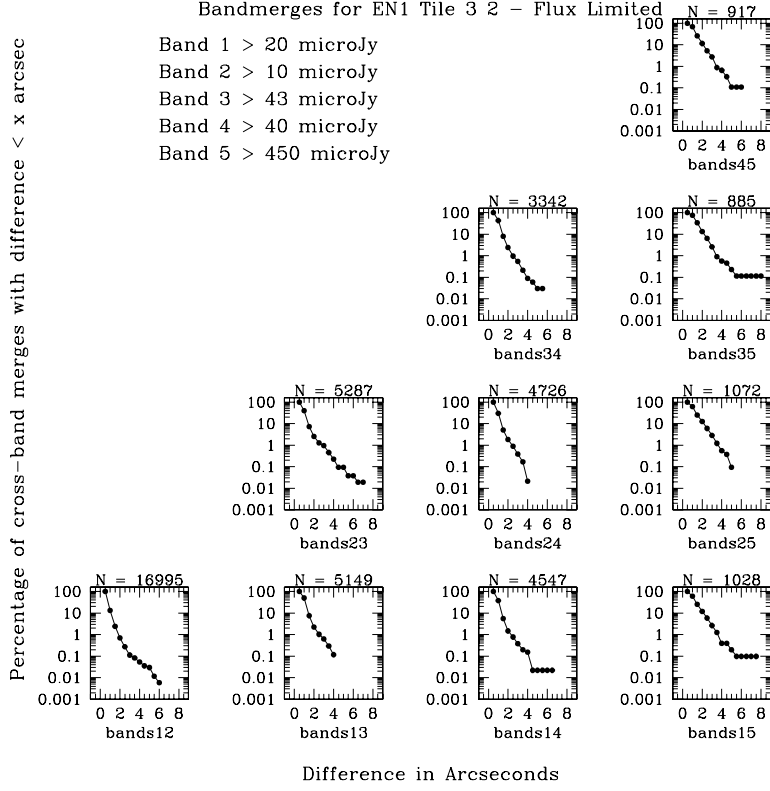
Fig. 35.— Cumulative distribution plots of the radial offsets between bandmerged positions in each band.
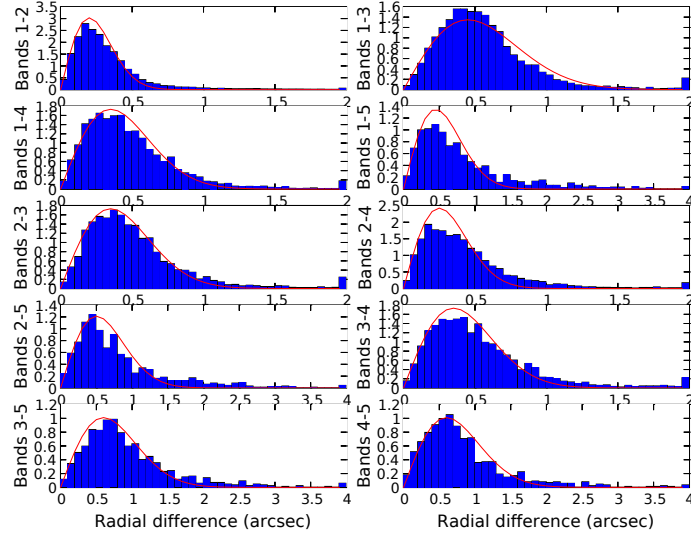
Fig. 36.— Histograms of radial offsets between bandmerged positions in each band.
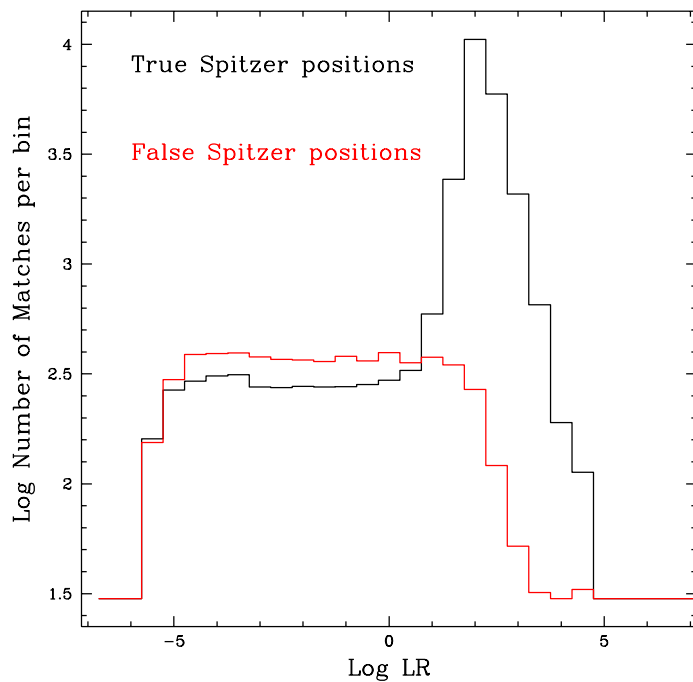
Fig. 37.— Distribution of likelihood ratios for true and false matches.
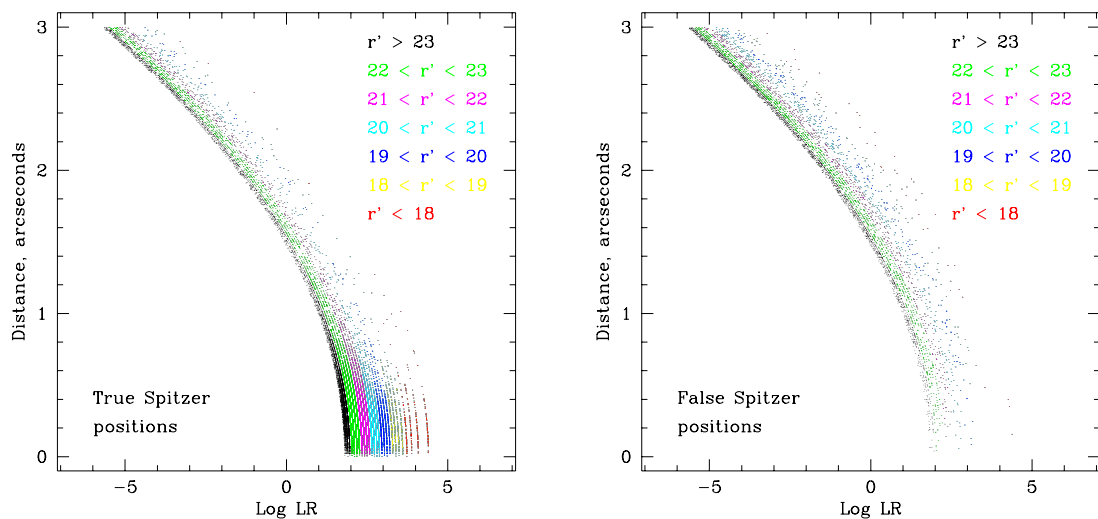
Fig. 38.— Likelihood Ratio for true (left) and false (right) as a function of separation and magnitude. At the "True" Spitzer positions, matches can be false as well as correct while at the "False" Spitzer positions matches are of course all false. Note that this figure is encoded with and should be viewed in color.
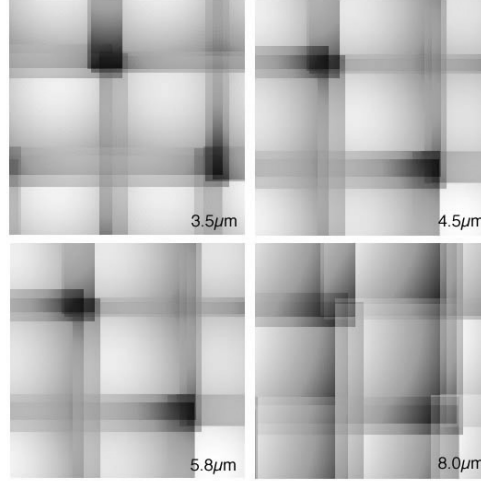
Fig. 39.— Mosaics of position-dependent gain correction for SWIRE. In general, the corrections are all well below 1%, except for small regions (appearing black or white in this figure) where the amplitude of the correction may reach 5-10%. The above figures are 5′ in size, equivalent to a single IRAC FOV.
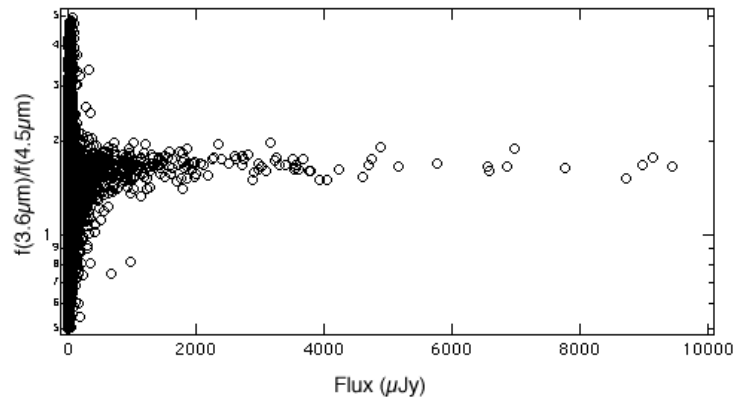
Fig. 40.— IRAC 3.6 and 4.5μm color-magnitude diagram. The stars have similar colors at these wavelengths.

9. Cautionary Notes

9.1. Incomplete Coverage at some Wavelengths and Apparent Null Detections

It is very important to note that the optical data does not completely cover the Spitzer fields; for example, 30% of the ELAIS-N1 field has no optical imaging data. **Thus a null-value in a given band may indicate lack of coverage rather than non-detection.** Users should use the supplied coverage flags to determine the meaning of a null value.

9.2. Bright Sources and Bright Source Artifacts

Very bright sources, usually stars, and not well handled by SExtractor as implemented for the SWIRE pipeline, therefore the user should not expect all bright stars to be present in the SWIRE V2.0 IRAC-24μm Catalog, and those stars that do appear may well have incorrect fluxes. SWIRE is an extragalactic survey and therefore no effort has been expended at this time to recover fluxes of bright stars.

Moreover bright stars give rise to numerous artifacts in their vicinity which can be extracted as sources. We have attempted to eliminate as many of these as possible, have flagged sources lying close to bright stars, and have used two-band detection as a requirement for making it into the catalog, but bright star-related artifacts may none-the-less remain in the IRAC-24μm Catalog.

9.3. Cosmic Rays

The IRAC detectors experience a cosmic ray hit rate of approximately one radhit per second per detector, each of which affects several pixels. While cosmic rays are removed from the data using outlier rejection, a few cosmic ray blemishes remain. These are particularly likely to occur in the case of radiation hits that strike pixels where an actual object is present. While the incidence of this is small, some selection criteria that specify unusual colors may result in selecting such objects. It is recommended that users visually inspect images of unusually-colored sources.

9.4. Duplication of Sources between Tiles

Limitations inherent to current computing resources forced us to process the IRAC data in the tiles described above. In order to avoid edge effects, the tiles were deliberately designed to have some degree of overlap. Source extraction was performed on these tiles. As a result of this overlap, the same source could appear in more than one tile. Removal of these duplicate sources was performed by assigning them to the tile whose center they were closest to. However, in some rare cases it is possible that a source may have been extracted on either side of the midline between tiles, and hence may appear twice.

9.5. Backgrounds

The backgrounds in the SWIRE images are not accurate and should not be considered measurements. IRAC cannot measure the true background, and the BCD images as delivered by the SSC have a background

which is the difference between the true background in the raw SWIRE images and the background at the north ecliptic pole. They additionally have small offsets resulting from the IRAC first-frame effect. As discussed in Section 5.2.1 each image therefore has it's median value forced equal to a model of the zodiacal background.

The MIPS-24 backgrounds have not been adjusted from the values in the BCD images delivered by SSC. We have not validated these values in any absolute sense. Owing to the nature of the MIPS-Ge detectors, the background values in the 70μm and 160μm maps are definitely not accurate measurements of the infrared background level.

Since the SWIRE survey is a cosmological survey geared towards measurement of small, compact objects, local background evaluation is used for all of the measurements. Thus, the fidelity of the background is not particularly important.

9.6. Photometry of Extended Sources

Users are warned that source extent relative to the PSF can be highly wavelength-dependent due to the large difference in PSF size with wavelength. Therefore **a source that is point-like in a long wavelength band can be extended at a shorter band**, even if the galaxy size is independent of wavelength.

9.7. Incomplete and Unreliable Bandmerges and Optical Cross-Identifications

Bandmerging the four IRAC bands together is a relatively straightforward process at the source densities encountered by SWIRE, but bandmerging the IRAC sources with 24μm sources is trickier because the PSF increases rapidly with wavelength, and because there exists a wide range of spectral shapes between the longest wavelength IRAC band, 8μm and 24μm. Therefore the bandmerge processor sometime fails to make the correct identifications. Once a given 24μm source is wrongly associated with an IRAC source, the correct 24μm source is left unmerged. We have mitigated this problem by eye inspection of all 24μm sources in the V2.0 release, but some problems may remain.

For the optical cross-identifications, we are reasonably confident that all potential matches between Spitzer and optical sources have been included in the $1.5''$ search radius, however this means that we have allowed in a significant number of unreliable matches with background sources. The V2.0 data products also provide a probability measure for each potential optical cross-identification.

Some Spitzer sources had more than one potential optical match. For the IRAC-24μm Catalog we have selected only one match to report; that with the largest goodness-of-match criterion, a parameter that is inversely related to separation. It is possible that the correct match has sometimes been deleted in favor of an incorrect one; specifically when the correct match to the Spitzer source is further from it than the selected match but is significantly brighter than the selected match (brighter galaxies have lower surface density than fainter ones).

9.7.1. Asteroids

Asteroids appear as a noticeable contaminant in the XMM-LSS field, which lies at low ecliptic latitude. Asteroids may be identified by their extraordinary redness - they often appear as 8μm only sources.

Asteroids, which may be present in one epoch of IRAC data, but not in the next, give rise to a peculiar artifact. Outlier detection during coaddition may reject the core of the PSF, but not the wings, resulting in small "rings" of extremely red emission at 8μm.

9.7.2. Straylight from Mira in the XMM-LSS field

The XMM-LSS field just skirted the extremely luminous star Mira, seen just to one side of tile 2_4. While the IRAC detectors never pointed at Mira itself, tiles 2_4 and 3_4 suffer from significant numbers of straylight artifacts. As a result, reliability of sources in these two tiles is lower than for the rest of the survey area. Additionally, scattered light in the Spitzer telescope produced several rings of scattered light nearly half a degree in diameter. Additional tests by the IRAC instrument support team at the SSC demonstrated that these rings are artifacts of the telescope.

10. Contributions

The SWIRE data processing effort, including pipeline design, was led by Jason Surace. Data processing strategy for the IRAC camera was led by Jason Surace. Dave Shupe has led the SWIRE MIPS processing plan. The overall data management pipeline and the IRAC processing pipeline was principally developed by Sandra Castro and Fan Fang, and is maintained and operated by Fan Fang. Data processing for MIPS 24μm has been undertaken by Frank Masci and Dave Shupe, in consultation with Deborah Padgett. Data processing for MIPS 70 and 160μ has been undertaken by Dave Frayer, Dave Shupe, Alejandro Afonso-Luis, C. Kevin Xu, and Donovan Domingue. The optical data processing effort was led by Eduardo Gonzalez-Solares and Tom Babbedge. Dave Shupe has overseen the bandmerging process. Data and database management and processing of the Spitzer-optical cross-identifications was undertaken by Tracey Evans. Anastasia Alexov was responsible for the mosaicking of the optical images onto the Spitzer tile system.

11. Acknowledgments

12.   References

Barbmy, P., & Lacy, M. "Pointing Refinement in IRAC Images", 2004

Berriman, G.B., Good, J.C., Curkendall, D., et al., 2002, "Montage: An On-Demand Image Mosaic Service for the NVO", ADASS

Bertin, E., & Arnouts, S, 1996, A&AS, 117, 393

Calabretta, M. R. & Greisen, E. W. 2002, A&A, 395, 1077

Chary, R. et al. 2004, ApJS, 154, 80

Ciliegi P. et al, 1999, MNRAS, 302, 222

Davoodi, P. et al. 2005, AJ, submitted

Diolaiti, E., et al. 2000, A&AS, 147, 335

Francseschini, A. et al. 2004, AJ, in press

Frayer, D. T., et al. 2005, submitted to ApJ

Gonzalez-Solares E. et al, 2004, MNRAS, in press

Hatziminaoglou, E. et al. 2004, AJ, in press

Irwin M., Detectors and Data Analysis Techniques for Wide Field Optical Imaging, 1999, Instrumentation for Large Telescopes: VII Canary Islands Winter School of Astrophysics, Cambridge University Press, Ed. Rodriguez Espinosa, J. M.; Herrero, A.; Sanchez, F.

Irwin, M. and Lewis, 2001, New AR, 45, 105

Gordon, K., et al. 2004, PASP, in press

Hall, P. & Mackay, C. D. 1984, MNRAS, 210, 979

Landolt, A., 1992, AJ, 104, 340

Lonsdale, C. J., et al., 2003, PASP, 115, 897

Lonsdale, C. J., et al., 200, ApJS, 154, 54

Makovoz et al., 2004, Astronomical Data Analysis Software & Systems proceedings, Pasadena, in preparation

Manners J.C. et al, 2003, MNRAS343, 293

McMahon, R., Walton, N., Irwin, M., et al., 2001, New AR, 45, 97

Oliver, S. et al. 2004, ApJS, 154, 30

Polletta, M. et al. 2005, AJ, in prep.

Rowan-Robinson M. et al, 2004a, MNRAS, 351, 1290

Rowan-Robinson, M. et al. 2004b, AJ, in press

Rutledge, R. E., Brunner, R. J., Prince, T. A and Lonsdale, C. J. 2000, ApJS, 131, 335

Serjeant S. et al, 2004, MNRAS, in press

Shupe, D.L. et al. 2005, in prep

Surace, J.A., et al. 2005, AJ, in prep
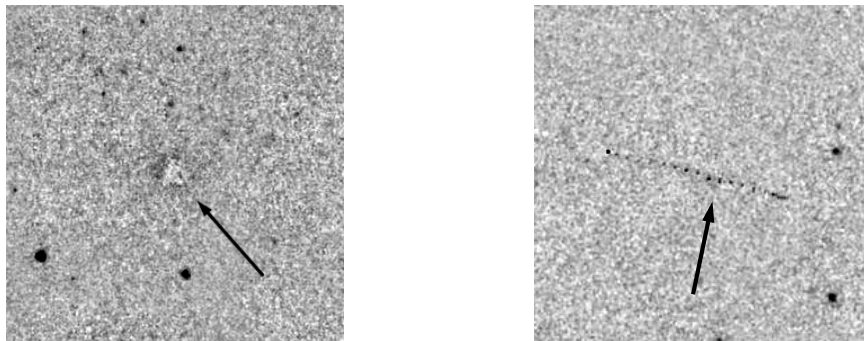
Vaisanen P. et al, 2002, MNRAS, 337, 1043

Fig. 41.— Examples of cosmic ray rejection errors. On the left is a 5.8μm image from the XMM-LSS field, showing a "comet"-like radhit, whose core has been partially rejected. On the right is an 8μm image, also from XMM-LSS, showing a partially rejected "track"-like feature. These two channels show the worst radhit effects due to the thick detector material. Similarly, this field has the worst radhit rejection due to the higher intrinsic background.
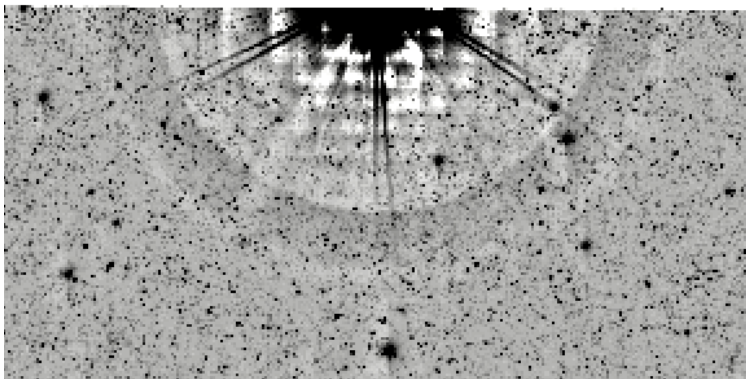

Fig. 42.— 3.6μm image of the upper part of the XMM-LSS field, showing Mira. The apparent large shells surrounding Mira are scattered light features and are not astrophysical (i.e. real). This figure is slightly over 1 degree across.